Polymer Brushes in Cylindrical Pores: Simulation versus Scaling Theory

D. I. Dimitrov[1], A. Milchev[2,3], and K. Binder[3]

[1] *Inorganic Chem. and Phys. Chem. Dept, Univ. Food Technol., Maritza Blvd. 26, 4002 Plovdiv, Bulgaria*
[2] *Instute for Chemical Physics, Bulgarian Academy of Sciences, 1113 Sofia, Bulgaria*
[3] *Institut für Physik, Johannes Gutenberg Universität Mainz, Staudinger Weg 7, 55099 Mainz, Germany*

February 6, 2008

Abstract

The structure of flexible polymers endgrafted in cylindrical pores of diameter D is studied as a function of chain length N and grafting density σ, assuming good solvent conditions. A phenomenological scaling theory, describing the variation of the linear dimensions of the chains with σ, is developed and tested by Molecular Dynamics simulations of a bead-spring model.

Different regimes are identified, depending on the ratio of D to the size of a free polymer $N^{3/5}$. For $D > N^{3/5}$ a crossover occurs for $\sigma = \sigma^* = N^{-6/5}$ from the "mushroom" behavior ($R_{gx} = R_{gy} = R_{gz} = N^{3/5}$) to the behavior of a flat brush ($R_{gz} = \sigma^{1/3}N$, $R_{gx} = R_{gy} = \sigma^{-1/12}N^{1/2}$), until at $\sigma^{**} = (D/N)^3$ a crossover to a compressed state of the brush, ($R_{gz} = D, R_{gx} = R_{gy} = (N^3D/4\sigma)^{1/8} < D$), occurs. Here coordinates are chosen so that the y-axis is parallel to the tube axis, and the z-direction normal to the wall of the pore at the grafting site.

For $D < N^{3/5}$, the coil structure in the dilute regime is a "cigar" of length $R_{gy} = ND^{-2/3}$ along the tube axis. At $\sigma^* = (ND^{1/3})^{-1}$ the structure crosses over to "compressed cigars", of size $R_{gy} = (\sigma D)^{-1}$. While for ultrathin cylinders ($D < N^{1/4}$) this regime extends up to the regime where the pore is filled densely ($\sigma = D/N$), for $N^{1/4} < D < N^{1/2}$ a further crossover occurs at $\sigma^{***} = D^{-9/7}N^{-3/7}$ to a semidilute regime where $R_{gy} = (N^3D/4\sigma)^{1/8}$ still exceeds D. For moderately wide tubes ($N^{1/2} < D < N^{3/5}$) a further crossover occurs at $\sigma^{****} = N^3D^{-7}$, where all chain linear dimensions are equal, to the regime of compressed brush.

These predictions are compared to the computer simulations. From the latter, also extensive results on monomer density and free chain end distributions are obtained, and a discussion of pertinent theories is given. In particular, it is shown that for large D the brush height is an increasing function of D^{-1}.

1   Introduction

Polymer brushes are layers of flexible linear polymers on substrate surfaces produced by endgrafting one chain end via a special chemical endgroup of the macromolecule

of colloid stabilization, lubrication, wetting, adhesion, etc. and hence they have found abiding interest. Polymer brushes also pose challenging theoretical problems, since the confinement due to the grafting at the substrates causes the emergence of many distinct characteristic lengths needed even to describe the structure of a single chain in a brush [6, 7, 8], and although the density profile of the monomers in the direction normal to the grafting surface has been studied since a long time ago [9, 10, 11, 12, 13, 14, 15, 16, 17], the degree to which this profile is understood quantitatively still is a subject of current discussion [18].

Note that the overwhelming part of the very rich literature on polymer brushes (see [1, 2, 3, 4, 5] for reviews) deals with brushes on planar flat surfaces only. Occasionally the problem of brushes on the outside of spherical particles {e.g. [19, 20, 21]} and on the inside of spherical cavities [20, 22, 23] was considered (as well as weakly curved flexible membranes, e.g. [24, 25]).

However, relatively little work has been done on grafted flexible polymers inside cylindrical pores (apart from a few comments in [20, 23] and a study of a single grafted chain in a tube [26], a problem that is closely related to the behavior of single non-grafted chains confined in tubes [27, 28]). We note that small mushrooms grafted to cylindrical pores were considered as a means to control electroosmotic flow [29].

In the present paper we intend to contribute to fill this gap, by presenting a study of polymer brushes grafted on the inside of cylindrical pores of radius R, varying also the chain length N and grafting density σ over a wide range. Such systems should be possibly also relevant in a biophysical context (cylindrical pores in biological membranes, blood vessels or other transport pipes or tube-like objects in biosystems, in which proteins or other biopolymers can be adsorbed), but this is outside of consideration here. Rather this paper is devoted to an understanding of the characteristic lengths that describe the configurations of the endgrafted chains in such a cylindrical confinement. In Sec. II, we formulate a (somewhat qualitative) scaling description, pointing out also the relation to the problem of non-adsorbed chains in cylindrical pores at various volume fractions of the monomers [27, 30, 31, 32, 33, 34]. In Sec. III, we describe the model used for our simulations to test this theory, while Sec. IV presents our numerical results for the linear dimensions of the chains. Sec. V describes results for the monomer density distribution across the channel, as well as corresponding results for the distribution function for the free chain end. Sec. VI then summarizes our conclusions.

2   Theoretical background: Scaling considerations

A very brief discussion of polymer brushes in cylindrical geometry was given in Appendix C of [23], however, many of the characteristic lengths relevant for our study were not given, and also a detailed derivation of the diagram describing the different regimes in the plane of variables R and σ was not presented; we give such a justification here, in order to make clear which underlying assumptions are made, and in order to be able to derive the new results on various characteristic lengths that are of interest here.

2.1   Mushrooms and Polymer Brushes on Flat Substrates

To set the scene, we recall the "blob model" of Alexander [9] and de Gennes [10] and its extension to deal with a nonuniform monomer concentration within a brush [6], see Fig. 1. For simplicity, all lengths will be measured in units of the effective segment length a, so the end-to-end distance of an ideal (Gaussian) chain containing

N segments simply is $\sqrt{N}$, and both grafting density σ and volume fraction ϕ are treated as dimensionless quantities. Only the good solvent regime is treated, and - as usual in the spirit of scaling approaches [35] - prefactors of order unity are suppressed throughout. Also the exponent ν describing the linear dimensions of a self-avoiding walk in $d = 3$ dimensions is simply approximated at the Flory value [36] $\nu = 3/5$, rather taking the more accurate value $\nu \approx 0.588$ [37, 38]. Thus an isolated polymer chain endgrafted at a planar wall, a "polymer mushroom", has the same gyration radii components as in the bulk,

$$R_{gx} = R_{gy} = R_{gz} = N^{3/5}. \tag{1}$$

Here, and in the following, we orient the z-axis normal to the grafting surface while the x and y-axes lie in the grafting plane (in the case of a a planar brush).

Considering then grafting densities σ large enough such that the individual mushrooms would significantly overlap, we recognize that (for $\sigma \ll 1$) we obtain a semidilute polymer brush, in which the screening length ξ is of the order of $\sigma^{-1/2}$, which then is taken as the blob-radius in Fig. 1. It is implied, that inside a blob excluded volume statistics persists, only n monomers from one chain are contained inside of such a blob, and no monomers of any other chains. Since $\sigma^{-1/2} = n^{3/5}$, in analogy to Eq. (1), we conclude that a blob contains $n = \sigma^{-5/6}$ monomers, and every chain contains $N_{blob} = N/n = \sigma^{5/6}N$ blobs. According to the Alexander [9]-de Gennes [10] picture, the chains in the brush form "cigars", i.e. they form linear chains of blobs stretched out along the z-axis (fig. 1, upper part), and hence the brush height h is of the same order as R_{gz}, namely

$$h = R_{gz} = \xi N_{blob} = \sigma^{1/3}N. \tag{2}$$

Taken literally, this "cigar" configuration would imply that $R_{gx} = R_{gy} = \xi = \sigma^{-1/2}$, which in reality is not the case: rather the chains in x and y-direction have a structure resulting from a random walk of blobs, i.e.

$$R_{gx} = R_{gy} = \xi N_{blob}^{1/2} = \sigma^{-1/12}N^{1/2}. \tag{3}$$

While the Alexander [9]-de Gennes [10] picture also implies that the monomer density profile $\phi(z)$ is essentially uniform for $z < h$, and the free chain ends are all in the outermost blob, i.e. in the region $h - \xi < z < h$, the structure in reality is much more complicated [6, 7, 8, 12, 13, 14, 15, 16, 17, 18]. Rather than staying constant, $\rho(z)$ smoothly decreases with increasing h (and in the strong stretching limit approximately is described by a parabolic variation, $\phi(z) = \phi(0)[1 - z^2/h^2]$). Due to this decrease of the monomer fraction $\phi(z)$ with the distance z from the grafting surface, also the screening length ξ is not a constant, but increases according to $\xi(z) = [\phi(z)]^{-3/4}$ [35]. From a self consistency consideration one can then estimate the diameter d_{fl} of the final blob as [6] $d_{fl} = N^{2/5}$. All these concepts have been verified by corresponding computer simulations [6, 7, 15, 16, 17, 18].

2.2 Cylindrical Tubes

We now consider a cylindrical tube of diameter D and length L. We orient the tube axis in y-direction and choose in this direction periodic boundary conditions.

We first note that there is a simple geometric relation between the grafting density σ of anchor points at the cylinder surface and the average volume fraction ϕ of monomers contained in the cylinder. Since the area of the cylinder surface is $A = \pi DL$, the total number of monomers $\mathcal{N}$ contained in the cylinder is

The cylinder volume being $V = \pi L D^2/4$, we find

$$\phi = \mathcal{N}/V = 4N\sigma/D \tag{5}$$

The condition that the maximum volume fraction that can be reached in a cylinder corresponds to a dense melt, i.e. $\phi = 1$, implies the following constraint for physically meaningful grafting densities σ

$$\sigma < D/(4N). \tag{6}$$

We first discuss the regime of extremely low grafting densities. For wide tubes, $D > N^{3/5}$, we still have mushrooms, i.e. Eq. (1) still holds. A more interesting regime occurs for narrow tubes,

$$1 < D < N^{3/5}, \tag{7}$$

where the chains form "cigars" stretched along the y-axis (Fig. 2). The situation for $\sigma \to 0$ closely resembles the case of non-grafted chains confined to very narrow tubes under good solvent conditions [27, 28]. One has $R_{gx} = R_{gz} = D$, while the longitudinal y-component R_{gy} is much larger. Assuming that the "cigar" configuration can be treated as an array of $N_{blob} = N/n$ blobs of diameter D, with n monomers per blob, $D = n^{3/5}$, we readily obtain

$$R_{gy} = DN_{blob} = DN/n = ND^{-2/3} \tag{8}$$

As it should be, for $D = N^{3/5}$ this yields a smooth crossover to $R_{gy} = N^{3/5}$.

Next we estimate how small the grafting density σ has to be in order that Eqs. (1) or (8) hold, respectively. The corresponding boundary in the $D-\sigma$ plane is obtained by the condition that the grafting density is such that the mushrooms or cigars just touch each other.

In the case of mushrooms, $D > N^{3/5}$, this boundary is reached for an overlap grafting density σ^* given by

$$\sigma^* = N^{-6/5}, \quad D > N^{3/5} \tag{9}$$

since each mushroom covers an area of order $N^{6/5}$ when one projects the monomer coordinates of the chain onto the grafting surface.

In the case of cigars, elongated along the y-axis, $D < N^{3/5}$, we simply have to equate the density ϕ in the tube to the density inside a cigar, using Eq. (8)

$$\phi^* = N/(D^2 R_{gy}) = D^{-4/3}. \tag{10}$$

This overlap density ϕ^* is easily converted into an overlap grafting density σ^* using Eq. (5),

$$\sigma^* = D\phi^*/(4N) = 1/(4ND^{1/3}), \ 1 < D < N^{3/5}. \tag{11}$$

Also in this case we note that for $D = N^{3/5}$ both expressions Eqs. (9), (11) for the overlap grafting density are of the same order, as it should be.

We now consider the behavior for $\sigma > \sigma^*$. In the regime where $D > N^{3/5}$ a crossover from mushroom to brush takes place, similar to the case of planar grafting surface. To leading order, Eq. (2) still holds. However, a strong compression of the brush sets in when the brush height h (and thus also R_{gz}) become comparable to the tube diameter. This yields a crossover grafting density σ^{**} separating a weakly compressed brush (described still by Eq. (2)) from a strongly compressed brush, with $R_{gz} = h = D$, for $\sigma > \sigma^{**}$,

In the regime of the compressed brush, the density ϕ of monomers is approximately uniform throughout the tube. Then the lateral linear dimensions are, similar as for chains in a semidilute solution in the bulk ($\xi = \phi^{-3/4}$), given as

$$R_{gx} = R_{gy} = \xi N_{blob}^{1/2} = \phi^{-1/8}N^{1/2} = (4\sigma)^{-1/8}D^{1/8}N^{3/8}, \sigma > \sigma^{**} \qquad (13)$$

At the boundary, $\sigma = \sigma^{**}$, Eq. (13) yields linear dimensions of order

$$R_{gx} = R_{gy} = D^{-1/4}N^{3/4} , \sigma = \sigma^{**}, \qquad (14)$$

and hence there occurs then again a smooth crossover to Eq. (3).

Finally, we address the behavior for $\sigma > \sigma^*$ in the narrow tube regime $D < N^{3/5}$. While for $\sigma = \sigma^*$ we have found "cigars" (Fig. 2) as described by Eq. (8) that just touch at their ends, we now expect "compressed cigars" in which the excluded volume interactions are partially screened. The polymer chains overlap themselves and near the cigar ends, neighboring cigars overlap each other. The screening length (blob radius) ξ then is smaller than the tube diameter, unlike the situation depicted in Fig. 2, namely

$$\xi = \phi^{-3/4} = (4N\sigma/D)^{-3/4}, \qquad (15)$$

where in the last step Eq. (5) was used.

For the range of grafting densities $\sigma^* < \sigma < \sigma^{***}$ (σ^{***} will be estimated below) we have compressed cigars with linear dimensions $R_{gx} = R_{gz} = D$ and linear dimensions $R_{gy} > D$ along the y-axis. Assuming that the volume $D^2 R_{gy}$ is of the same order as the total volume taken by all the blobs of a chain, $\xi^3 N_{blob} = N\xi^{4/3}$, one finds

$$R_{gy} = D^{-2}N\xi^{4/3} = D^{-2}N\phi^{-1} = 1/(4\sigma D) \qquad (16)$$

The result $R_{gy} = D^{-2}N\phi^{-1}$ is identical to the corresponding result for non-grafted chains confined to narrow tubes [30, 34], as expected. In this quasi-one-dimensional situation the "cigars" are laterally compressed, each chain overlaps itself to some extent (excluded volume is respected only up to the length ξ, Eq. (15)), but neighboring chains are still essentially segregated from each other and overlap only near the ends of the "cigar".

Now the boundary σ^{***} of this regime can simply be estimated from the condition that R_{gy}, Eq.(16), equals the result in the compressed brush regime, Eq. (13), which yields

$$\sigma^{***} = \frac{1}{4}N^{-3/7}D^{-9/7} \qquad (17)$$

Note that for $D = N^{3/5}$ this boundary starts at $\sigma^{***} = (1/4)N^{-6/5}$, i.e. it splits off from the boundary σ^* in the (D, σ) plane (Fig. 3). The other end of this boundary is reached for the condition $\phi = 1$, i.e. $4\sigma^{***} = D/N$ (Eq. (5)) and hence $D = N^{1/4}$. This means, for ultra-narrow tubes (defined by the condition $D < N^{1/4}$) Eq. (16) holds from $\sigma = \sigma^*$ up to $\sigma = D/4N$, so the boundary σ^{***} cannot be reached.

For tubes that are not ultra-narrow ($D > N^{1/4}$) one encounters at σ^{***} a crossover to a regime of semi-diluted cigars where now two of the three linear dimensions $R_{gx} = R_{gz} = D$, while the third linear dimension, R_{gy}, is given by Eq. (13). However, the cigars now start to overlap more and more, until at a grafting density σ^{****} the "natural size" R_{gy} of a chain in a semidilute solution of density ϕ reaches D,

$$R_{gy} = \xi N_{blob}^{1/2} = \phi^{-1/8}N^{1/2} , \quad \sigma^{***} < \sigma < \sigma^{****}. \qquad (18)$$

While in the regime described by Eq. (18) R_{gy} still exceeds D, and therefore the linear dimension of a chain in y-direction exceeds the other linear dimensions, we

denote this regime as "overlapping cigars". The grafting density σ^{****} is found from the condition that $R_{gy} = D$, and hence

$$D = \xi N_{blob}^{1/2} = (4N\sigma/D)^{-1/8}N^{1/2} \ , \ \sigma^{****} = \frac{1}{4}N^3 D^{-7} \tag{19}$$

For $\sigma^{****} < \sigma < D/4N$ we enter the same region of compressed brush that we have already encountered for $D > N^{3/5}$ for $\sigma^{**} < \sigma < D/4N$. The line σ^{****} starts in the (D, σ) plane also for $D = N^{3/5}$ at the point $\sigma = \frac{1}{4}N^{-6/5}$, i.e. at σ^*, and ends for $\phi = 1(\sigma = D/4N)$ at the diameter $D = N^{1/2}$ (Fig. 3).

The behavior of the brush in a tube becomes somewhat more transparent if we discuss it in terms of the scaled variables $\tilde{D} \equiv D/N^{3/5}, \tilde{\sigma} \equiv \sigma N^{6/5}$, since then (in the dilute and semidilute regime) the dependence on the chain length is absorbed completely. Fig. 4 shows qualitatively the dependence of the chain linear dimensions: For $\tilde{D} > 1$ the scaled radius $\tilde{R}_{gz} \equiv R_g/N^{3/5}$ crosses over from unity at $\tilde{\sigma} = 1$ to the power law $\tilde{\sigma}^{1/3}$ and at $\tilde{\sigma} = \tilde{\sigma}^{**} = \tilde{D}^3$ to $\tilde{D}$, while the other components of the radius, $\tilde{R}_{gx} = R_{gx}/N^{3/5}$, $\tilde{R}_{gy} = R_{gy}/N^{3/5}$ cross over from unity at $\tilde{\sigma} = 1$ to the power law $\tilde{\sigma}^{-1/2}$ and at $\tilde{\sigma}^{**}$ (where $\tilde{R}_{gy} = \tilde{D}^{-1/4}$) a further crossover to $(\tilde{D}/\tilde{\sigma})^{1/8}$ occurs.

Similarly, for $\tilde{D} < 1$ the radius $\tilde{R}_{gy}$ is $\tilde{D}^{-2/3}$ for small $\tilde{\sigma}$ and crosses over at $\tilde{\sigma}^* = \tilde{D}^{-1/3}$ to a power law $(\tilde{\sigma}\tilde{D})^{-1}$. For $\tilde{D} < N^{-4/15}$ this is the only crossover that occurs, while for larger $\tilde{D}$ additional crossovers are found at $\tilde{\sigma}^{***}$ (and $\tilde{\sigma}^{****}$, if $\tilde{D}$ exceeds $N^{-1/10}$) with $\tilde{\sigma}^{***} = \tilde{D}^{-2}$, $\tilde{\sigma}^{****} = \tilde{D}^{-7}$.

For $\tilde{\sigma} > \tilde{\sigma}^{***}$ we have $\tilde{R}_{gy} = \tilde{D}$, but only at $\tilde{\sigma} = \tilde{\sigma}^{****}$ the radius of a chain in a bulk semidilute solution of density $\tilde{\phi}$ corresponding to $\tilde{\sigma}$ would be of order $\tilde{D}$ and one goes over to compressed brush behavior where $\tilde{R}_{gy}$ decreases to linear dimensions smaller than $\tilde{D}$, namely $\tilde{R}_{gy} = (\tilde{D}/\tilde{\sigma})^{1/8}$, as above.

Note that in the case $\tilde{D} < 1$ the behavior of the brush in the tube in many aspects is similar to the behavior of non-grafted chains in a tube, as discussed by [30, 34]. One can see this converting σ to ϕ, using Eq. (5); however, for the latter problem the crossover at $\tilde{\sigma}^{****}$ has a different meaning: then all three linear dimensions $\tilde{R}_{gx}$, $\tilde{R}_{gy}$, $\tilde{R}_{gz}$ are smaller than $\tilde{D}$, given by $\tilde{R}_{g\alpha} = (\tilde{D}/\tilde{\sigma})^{1/8}$, for $\alpha = x, y, z$ while for $\tilde{\sigma} < \tilde{\sigma}^{****}$ we have $\tilde{R}_{gx} \equiv \tilde{R}_{gz} = \tilde{D}$ for the non-grafted confined chains. For the grafted confined chains, we also have $\tilde{R}_{gx} = \tilde{R}_{gz} = \tilde{D}$ in this regime, but $\tilde{R}_{gx}$ and $\tilde{R}_{gz}$ may differ from each other by factors of order unity (which are suppressed here in our scaling description), while for the non-grafted chains these components are identical by the symmetry of the problem. For $\tilde{\sigma} > \tilde{\sigma}^{****}$, however, there is a difference on a scaling level, since the grafting of the chain ends at the walls creates an elastic energy in the brushes, causing chain stretching in the normal direction (z), and $\tilde{R}_{gz}$ stays at its (maximal) value which is of order $\tilde{D}$. Finally, we note that in the scaling diagram of Manghi et al. [23] the line corresponding to $\tilde{\sigma}^{***}$ was not included. From Fig. 4, however, it is evident that an intermediate regime between the isolated cigars ($\tilde{R}_{gy} = \tilde{D}^{-2/3}$) and the semidilute regime ($\tilde{R}_{gy} = (\tilde{D}/\tilde{\sigma})^{1/8}$) is mandatory to provide a smooth crossover of the linear dimension $\tilde{R}_{gy}$ and $\tilde{\sigma}^*$. Note also, that on the crossover line $\tilde{\sigma}^{****}$ where $\tilde{R}_{gy} = \tilde{D}$ and hence all linear dimensions are of order $\tilde{D}$, the behavior of $\tilde{R}_{gx}$ changes: we have $\tilde{R}_{gx} = \tilde{D}$ for $\tilde{\sigma} < \tilde{\sigma}^{****}$ but $\tilde{R}_{gx} = \tilde{R}_{gy} = (\tilde{D}/\tilde{\sigma})$ for $\tilde{\sigma} > \tilde{\sigma}^{****}$.

3 Model and some Remarks on Simulation Methods

Being interested in phenomena of mesoscopic length scales of order $10 nm$ (or more) where chemical detail only enters into prefactors of various quantities, and a scaling

where atomistic details are not included is mandatory for the sake of computational efficiency of our computer simulation[39, 40, 41, 42, 43]. There is compelling evidence that the generic properties of flexible polymers in solution and melt can be described by simple bead-spring models where each bead may represent a few chemical monomers along the chain backbone[39, 47], and actually such models have been used for previous simulations of polymer brushes[3, 4, 15, 18, 48, 49] successfully.

In this bead-spring model the interactions between the beads modelling the monomer units are described by a Lennard-Jones (LJ) potential that is truncated at r_c and shifted there to zero,

$$U_{LJ}(r) = 4\varepsilon \left[\left(\frac{\sigma_{mm}}{r} \right)^{12} - \left(\frac{\sigma_{mm}}{r} \right)^6 \right] + \varepsilon \frac{127}{4096}, \ r < r_c \tag{20}$$

where $r_c = 2^{7/6}\sigma_{mm}$. Here ε characterizes the strength and σ_{mm} the range of the LJ-potential. Note that the minimum of U_{LJ} occurs at $r_{min} = 2^{1/6}\sigma_{mm}$, without the additive constant $\varepsilon \frac{127}{4096}$ the depth of this minimum would be $U_{LJ}(r = r_{min}) = -\varepsilon$. Due to the shift of U_{LJ} at $r_c = 2r_{min}$, the potential in Eq. (20) is continuous at all $r > 0$.

In addition, monomers bonded to each other as nearest neighbors along a polymer chain interact with a finitely extensible nonlinear elastic (FENE) potential [44]

$$U_{FENE}(r) = -15\varepsilon \left(\frac{R_0}{\sigma_{mm}} \right)^2 \log \left(1 - \frac{r^2}{R_0^2} \right), \ R_0 = 1.5\sigma_{mm}. \tag{21}$$

The choice of these parameters ensures that the minimum of the total potential between two bonded monomers along the chain occurs for [45, 46] $r \approx 0.96\sigma_{mm}$, distinct from $r_{min} \approx 1.12\sigma_{mm}$. This misfit between the two distances ensures that there is no tendency of monomers to form a simple crystal structure even if the density is very high and/or the temperature is rather low. However, in the present paper we shall consider only temperatures in the good solvent regime of our model. This means, the temperature T must exceed the Θ-temperature, which for the present model has been established as [47] $k_B T/\epsilon \approx 3.3$. Thus, we choose $k_B T/\epsilon = 4$ for our simulation. To simplify the notation we choose $k_B \equiv 1$ and take $\varepsilon \equiv 1$ and $\sigma_{mm} = 1$ as our units of energy and length, respectively.

The grafting wall is represented by atoms forming a triangular lattice, wrapped around a torus by a periodic boundary condition. This choice of wall is inspired by carbon nanotubes. However, the potential with which effective monomers and wall atoms interact is chosen to be the same as the monomer-monomer potential, Eq. (20). Also, the wall atoms are fixed in the rigid positions of an ideal crystal lattice. This guarantees that no monomer can cross the wall of the tube and get out of it. Of course, the coarse-grained nature of our polymer model would make a chemically realistic description of a cylindric pore meaningless. The polymers are grafted hexagonally on a cylinder with radius $R-1.0$, thus defining a grafting density σ while the tube atoms are placed a little further - on a cylinder with radius R. It might be more realistic, of course, to choose randomly distributed grafting sites, however, the experience with flat brushes[17] shows that it makes little difference whether the grafting sites are distributed regularly or at random. The size of the simulation box along its axis y is L_y and the number of static particles, forming the tube N_{tube}, are different for simulation of tubes with different radii R: for $R = 15$, $L_y = 81.62$, $N_{tube} = 1024$; for $R = 21$, $L_y = 76.18$, $N_{tube} = 2400$; and for $R = 31$: $L_y = 67.47$, $N_{tube} = 1240$.

Simulations are performed by a standard leapfrog algorithm at constant temperature, maintained by a Nosè-Hoover thermostat [48], combined with a simple "hot

"particle temperature" differs from the average value too much. Choosing the mass of an effective monomer as $m \equiv 1$, the MD time unit is $t_0 = (\sigma_{mm}^2 m/48\varepsilon)^{1/2}$, and the time step of integration $\delta t = 0.0005 t_0$.

Particular care has to be devoted to the construction of the initial configuration of the grafted polymers and their equilibration. The construction of the starting configuration for given (N, σ, R) begins with the growth of the chains in a tube with radius $R_{init} = 2R$ and $N = N_{max}$, where N_{max} is the number of monomers in the longest chain, investigated for these σ and R. After placing the first monomer at the grafting site, each consecutive monomer is placed at a distance $0.75 R_0$ from the preceding one along a direction $\mathbf{r} = 2.0 * \mathbf{e_{0z}} + \mathbf{e_{rand}}$ where $\mathbf{e_{0z}}$ is a unit vector, pointing radially from the grafting site to the tube axis, and $\mathbf{e_{rand}}$ is a unit vector oriented at random. After an initial equilibration of this system for about 10^5 MD steps, we rescale the system radius to the final system with desired radius R and again let the system equilibrate for 10^5 steps. From the final configuration of this system, by cutting systematically the polymer chains to different values of N, we obtain the "starting configurations", which we additionally equilibrate for about 3.10^5 steps and (depending on N and σ) then collect statistics during the following $2.10^5 - 4.10^5$ integration steps. Typical examples of equilibrated brush configurations in this cylindrical geometry are shown in Fig. 5. For all three tube diameters $D = 30, 42$, and 62 as well as for chain lengths $8 \leq N \leq 64$ we then sample brush profiles and components of gyration radius, R_g, and end-to-end distance vectors of the chains, R_e, for seven different grafting densities σ. In our simulations we have refrained, however, from creating elongated cigar-like configuration, cf. Fig. 2b, since the distribution $\rho(y)$ of R_e is expected to be bimodal (that is, the center-of-mass of the chains is either to the left, or to the right of the grafting site, as shown in Fig. 2b). The equilibrium $\rho(y)$ is expected to produce a pronounced minimum above the grafting site at $y = 0$ and, therefore, a well equilibrated distribution $\rho(y)$ would imply that the chain end passes the coordinate $y = 0$ many times which can hardly be possible within the typical time interval of a MD simulation.

4 Linear dimensions of chains in brushes in cylindrical pores

In order to test our model and check that for the rather short chain lengths used in the present work (typically $8 \leq N \leq 64$) results are obtained that one can compare to the theoretical predictions, which really address the asymptotic regime $N \rightarrow \infty$ only, we first present data for brushes on flat substrates in Figs. 6, 7. One recognizes that for small σ, such as $\sigma \approx 0.0115$, the linear dimensions in the z-direction, perpendicular to the substrate, and in the y-direction, are rather similar for the range of chain lengths that is studied, but the effective exponents ν_{eff} in the relations $\langle R_{gy}^2 \rangle \propto N^{2\nu_{eff}}$, $\langle R_{gz}^2 \rangle \propto N^{2\nu_{eff}}$ somewhat differ from the theoretical value in the mushroom regime, $\nu = 3/5$ (Eq. (1)). For the grafting density $\sigma \approx 0.1039$, however, we recognize that the scaling behavior of the chain linear dimensions strongly depends on direction, $\langle R_{gz}^2 \rangle \propto N^{1.86}$ while $\langle R_{gy}^2 \rangle \propto N^{1.16}$, and approaches the theoretical behavior that is expected for much larger N, $\langle R_{gx}^2 \rangle \propto N$ while $\langle R_{gz}^2 \rangle \propto N^2$ (Fig. 6c). Since comparatively short chains are used, it would be premature to expect that one reproduces the asymptotic exponents of the scaling theory precisely. Also the dependence of both $\langle R_{gy}^2 \rangle$ and $\langle R_{gz}^2 \rangle$ on σ is roughly compatible with the predicted power laws (Eqs. (2), (3)). Of course, for polymer brushes on flat substrates it would be easier to equilibrate significantly longer chains: e.g., [48] used $50 \leq N \leq 200$ for a closely related model, and [18] used $16 \leq N \leq 512$. Even then

However, for the brushes in the cylindrical pores good equilibration is significantly more difficult; therefore we restrict the present work to relatively short chains.

Thus, it cannot be a surprise that in the scaling plots (Figs. 7a,b) a perfect collapse on master curves is not obtained, and rather some systematic deviations due to corrections to scaling are clearly apparent. Such corrections to scaling are presumably also responsible for the fact that the effective exponents ν_{eff} in the mushroom regime of Figs. 6b,c deviate from their theoretical value. Note also that in the present work a somewhat more restricted range of grafting densities is studied than in [18], where much lower grafting densities were included to ensure to reach the mushroom regime fully. Our data in Fig. 6 even for the smallest values of σ are already affected a little bit by the crossover towards the brush regime, since this crossover occurs rather gradually.

In [18] also the problem was discussed that for temperatures not too far from the Theta temperature the excluded volume interaction on the scale of a blob diameter may be so weak that then in the regime of high grafting densities inside of a blob gaussian chain statistics still holds. As a consequence, then a further crossover that occurs for large $\tilde{\sigma}$ under good solvent conditions has been identified. However, this crossover gives rise to rather small and subtle effects, and hence can be safely ignored in the present context.

We now turn to our data for brushes in cylindrical pores. Figs. 8-10 present the linear dimensions $\langle R_{gz}^2 \rangle$ and $\langle R_{gy}^2 \rangle$ for three choices of the pores diameter, $D = 30$, 42, and 62. For the narrow pore ($D = 30$), one sees a weak increase of $\langle R_{gz}^2 \rangle$ with σ for small N, while for larger N no longer any increase occurs. This behavior is in marked contrast with the behavior of the brush on the flat substrate. In contrast, $\langle R_{gy}^2 \rangle$ decreases with σ monotonously, while the theoretically predicted double crossover (Fig. 4) is not seen. For the wider tube, such as $D = 62$, one still sees a more pronounced increase of $\langle R_{gz}^2 \rangle$ with σ, but if one would fit a power law to this increase, the effective exponent would be distinctly smaller than the theoretical value $2/3$, that should still be observable in an intermediate regime of σ, see Fig. 4. However, since the crossovers (from the mushroom regime to the brush and from the brush to the compressed brush) do not occur at sharply defined values of σ, but are rather expected to be smeared out over a range of values σ that may be a full decade or even more. Therefore instead of the two "kinks" in Fig. 4 a smooth gradual increase with σ is noted. Similarly, when we study $\langle R_{gz}^2 \rangle$ as a function of N (Fig.10c), one can still see straight lines on the log-log plot, but the observed effective exponents are somewhere in between $2\nu = 1.2$ and 2, indicating the onset of compression due to the confinement of the brush in the tube. However, such effective exponent which simply reflect slow crossovers do lack any deep physical significance, of course.

Motivated by the scaling analysis of Sec. II, we discuss the extent to which the chain length dependence can be absorbed in scaling plots of $\tilde{R}_{gy}$ and $\tilde{R}_{gz}$ versus $\tilde{\sigma}$ (Fig. 11). Of course, only for $\tilde{D} > 1$ the first crossover from mushrooms to the almost unperturbated brush is expected to stay unaffected by D. Since varying N at fixed D means that different values of $\tilde{D}$ occur, the positions of the various other crossovers in Fig. 11 do depend on N via the N-dependence of $\tilde{D}$. So we expect that the curves for $\tilde{R}_{gz}^2$ vs $\tilde{\sigma}$ at large enough $\tilde{\sigma}$ start to split off from the master curve that describes both the mushroom and brush regime and saturate at plateaus corresponding to the different values of $\tilde{D}$. Some evidence for the splaying out of the curves on the right hand side of the scaling plot for $\tilde{R}_{gz}^2$ can indeed be seen in Fig. 11. However, for the parameters accessible in our study the crossovers at $\tilde{\sigma}^* = 1$ and at $\tilde{\sigma}^{**} = \tilde{D}^3$ are too close together, so the intermediate regime where $\tilde{R}_{gz}^2 = \tilde{\sigma}^{2/3}$ is never clearly realized. In fact, in order to clearly separate these crossovers, one would

small N corrections to scaling come into play also and obscure the behavior further. Part of our data falls into the region $\tilde{D} < 1$, where a different pattern of crossover behavior applies, but again the different regions are clearly separated only if $\tilde{D} \ll 1$ is achieved. We could not reach this region due to difficulties of equilibration.

Thus Fig. 11 does not give strong evidence for the scaling theory of Sec. II: clearly these scaling considerations are useful only for the special limit where both N and D are very large, σ being very small, so that $\tilde{\sigma}$ can be varied over many decades, as well as $\tilde{D}$. This limit is not easy to reach in our simulations. Nevertheless the scaling theory gives a useful orientation: note that the data for the scaled quantities $\tilde{R}_{gy}^2$ and $\tilde{R}_{gz}^2$ in Fig. 11 show remarkably little variations in spite of the fact that both N and σ are varied over about an order of magnitude each.

5 Monomer density and chain distribution across a cylindrical pore

We start this section again with a brief glimpse on the behavior of our model in the limit of a flat grafting surface - Fig. 12. As expected, one sees a smooth decay of the monomer density profile $\phi(z)$ with increasing distance z from the surface. When N increases, the height h of the brush (region where $\phi(z)$ is appreciably nonzero) strongly increases (Fig. 12a). Since from Eq. (2) we expect that $h \propto N$, it is interesting to plot $\phi(z)$ against a rescaled coordinate z/N (Fig. 12b). One can see that for large N the curves indeed converge smoothly towards a master curve, and this master curve resembles the simple parabolic shape predicted by the selfconsistent field (SCF) theory in the strong stretching limit [12, 13, 14]

$$\phi(z) = \phi(0)[1 - (z/h)^2] \quad N \to \infty, \ \sigma \to 0, \ N\sigma^{1/3} \text{ finite} \tag{22}$$

Eq. (22) implies a nonzero intercept $\phi(0)$, while the actual $\phi(z \to 0) \to 0$, of course (Fig. 12): so the $\phi(0)$ of Eq. (22) is interpreted as an extrapolation of the flat part of the profile; also $\phi(z) \equiv 0$ for $z > h$, which for finite N is not true. However, numerical implementations of SCF theory that do not invoke the strong stretching limit, such as the Scheutjens-Fleer theory [51], can describe the smooth decay of the tail of the profile $\phi(z)$ for $z > h$ [52], but this is not attempted here. In order to provide a precise definition of h from the observed profiles $\phi(z)$, such as shown in Fig. 12, we follow previous practice (e.g. [18]) to use the first moment $\langle z \rangle$,

$$h = \frac{8}{3}\langle z \rangle, \quad \langle z \rangle = \int\limits_0^\infty z\phi(z) / \int\limits_0^\infty \phi(z)dz. \tag{23}$$

It is easily checked that Eqs. (22) and (23) are compatible with each other, but Eq. (23) is generally applicable. The insert of Fig. 12 gives evidence that the scaling regime $h \propto N$ has not yet fully been reached by our rather short chains, but at least there is evidence that the chains are stretched away from the surface. Similar data have been generated by many previous simulations on various models [3, 6, 15, 16, 17, 18]. The delta-function like peak for the first monomer (at $z = 1.0$) simply is due to the fact that the wall atoms forming the flat surface are at a fixed distance $z = 1.0$ away from the first monomer of the chain.

We also draw attention to the weak oscillations in the density profile ("layering") that is visible for small z. Such effects arise from the "packing" of monomers near the grafting surface, which resembles a hard wall. Such packing effects are neither described by the scaling theory of Sec. II nor the SCF theory, of course.

Also the distribution function $\rho(z)$ of the end monomers is of interest (Fig. 12c).

prediction of the Alexander [9] - de Gennes [10] picture, according to which the chain ends are all localized at a distance $z \approx h$ from the grafting surface. According to the strong stretching limit of SCF theory, however, one would predict a distribution that is spread over the entire brush but vanishes at $z = h$ with a divergent slope [12],

$$\phi_e(z) \propto z[1 - (z/h)^2]^{1/2}, \ N \to \infty, \ \sigma \to 0, \ \sigma^{1/3}N \text{ finite} \qquad (24)$$

From Fig. 12c it is clear that our data do not reach the strong stretching limit of the SCF theory, however.

For polymers grafted to a flat wall it would be possible to simulate much longer chains, of course, and, in fact, in [18] for a closely related model (perfectly flat wall with no corrugation whatsoever and using an integrated Lennard-Jones-type repulsive wall potential) chain lengths up to N = 512 were studied. However, even for the largest chains the strong stretching limit of the SCF theory was not reached. Since the main interest of the present paper concerns chains in cylindrical tubes, and for this case it is probably not feasible experimentally to graft extremely long chains at the tube walls, we shall not emphasize the comparison with the strong stretching limit of the SCF theory in the present paper; just as the scaling considerations of Sec. 2 it is useful for a first orientation, but one cannot rely on its quantitative details in the present case.

After this prelude on the density profiles for the well-studied case of polymer brushes grafted to planar substrates we turn to our results on the profiles in cylindrical pores, Figs. 13-16. While for short chains (such as $N = 8, 12, 16$) and low grafting densities these density profiles are typical of mushroom behavior, for larger N one quickly reaches a state where the whole cylindrical brush is more or less uniformly filled with monomers. In this limit the density of end monomers reaches a maximum near the tube axis, but in comparison with the brushes on flat substrates (Fig. 12) the distribution of the end monomers is more uniform. Thus the approximation of Sevick [20] assuming a delta-function distribution of chain ends (like in the Alexander [9]-de Gennes [10] model) obviously is not accurate, at least for the parameter range accessible in our simulations. At this point we recall that Sevick [20] predicts that the brush height h decreases with increasing inverse cylinder diameter D monotonously, while Milner and Witten [53] on the basis of their SCF theory suggest that the brush height h increases with $1/D$ (for small enough $1/D$). The interpretation for the latter result is that in the cylindrical pore the blob diameters get smaller with increasing distance z from the grafting surface when $1/D$ increases, since the volume available for the blobs decreases, and hence the tendency of the brush towards stretching is more pronounced in the outer region of a brush in a cylinder than for a brush at a flat substrate. Of course, when h and $D/2$ become comparable, the opposite tendency of compressing the brush due to the confinement will outweigh this increase of h that may be present for small $1/D$.

Again we emphasize that the grafted monomer (adjacent to the wall of the tube) is at a fixed distance $\Delta r = 1$ inside of the atoms forming the walls of the tube, which are at the radial distance $r = R$ from the tube axis. The sharp spike at $r = R - 1$ in Figs. 13a, 14a, 15a, 16a hence is always a representation of the delta function corresponding to the monomer adjacent to the rigid wall, at this fixed distance $\Delta r = 1$ inside of it. However, other monomers of the chain can come closer to the wall, when the chain bends back to the grafting wall. Therefore one finds a nonzero $\phi(r)$ in between $r = R - 1$ and $r = R$, as is clearly seen in Figs. 13a and 14a.

When the chain length N is small enough (and/or the tube diameter D is large enough), both $\phi(r)$ and $\rho(r)$ are essentially zero for $r \to 0$. The pore center then is still free of monomers, and Figs. 13 - 16 then contain also the full information on the distribution of the monomers as a function of the radial distance *from the*

grafting wall, r', we simply can transform from r to z via $r' = D/2 - r$. However, when either N gets larger or D gets smaller (or both), these distributions $\phi(r)$ and $\rho(r)$ get nonzero for $r \to 0$. This means that then distances larger than $D/2$ become possible {cf. Fig. 2(a)}. Then each value of r actually contains two entries for r', namely

$$r' = D/2 - r \text{ , for } r' < D/2, \text{ and } r' = D/2 + r, \text{ for } r' > D/2. \qquad (25)$$

The choice $r' = D/2 + r$ has to be used when the monomer lies in the upper hemicylinder with respect to the grafting site taken as the lowest point of the lower hemicylinder. Thus the tube axis in the simulation is at $r' = R = D/2$, since we arbitrarily defined $r = R - 1$ to be the position of the first monomer and put the wall at the radial distance $r = R$ from the tube axis.

Because of this ambiguity, it is also of interest to analyze separately the distribution functions $\phi(r')$ and $\rho(r')$. Fig. 17 gives an example (more details will be given in a forthcoming publication). Of course, for the cases which $\phi(r \to 0) \to 0$ and $\rho(r \to 0)$ the curves plotted in Fig. 17a are identical to those of Fig. 13, only now left and right is interchanged and the origin of the coordinate system shifted. However, this is not so in the cases where $\phi(r \to 0)$ and $\rho(r \to 0)$ are nonzero: we now see that $\phi(r')$ and $\rho(r')$ look qualitatively very similar to corresponding curves for brushes at flat walls. In particular, there is no singular behavior at the center of the tube, at $r' = R$ all curves are perfectly smooth. Also the distribution of chain ends $\rho(r')$ is perfectly smooth at this distance $r' = R$ and carries considerable weight for distances $r' > R$ if N is sufficiently large (and/or D sufficiently small), as Fig. 18b shows.

It is also of interest to examine the distribution of the chain end $\rho(y)$ as a function of the lateral coordinate y, parallel to the tube axis (Fig. 18). One can see that the width of this distribution does not depend much on the grafting density, and is largest for the smallest grafting density. No evidence for bimodal distributions, that are expected for narrow tubes and long enough chains due to the cigar-like configurations is found for the parameter range investigated, however.

The profiles $\phi(r')$ can be used to calculate the first moment $\langle r' \rangle$, from $\langle r' \rangle$ one obtains the brush height h, making use of Eq. (23). Fig. 19 shows a plot of the reduced height, h/N, versus N for $D = 42$ and $D = 62$ and two different grafting densities. A first important conclusion which one may draw upon inspection of Fig. 19 suggests that the brush height *grows* with increasing curvature of the tube, in contrast to the basic assumption in Sevick's theory [20]. Evidently, when the tube diameter diminishes the monomer density grows, cf. the inset of Fig. 19 where also the monomer density profile for a flat substrate, that is, zero curvature, is displayed. Clearly, as the density grows, the excluded volume interactions "push" the brush height toward the tube axis. As shown in Fig. 19, this effect is seen irrespective of particular grafting density σ. At higher σ, however, one can readily see that beyond a certain chain length ($N = 32$ for $D = 42$, and $N = 40$ for $D = 62$) the ratio h/N reaches a plateau, as expected on the ground of Eq. (2) whereas for the lower grafting density, $\sigma = 0.03$, the onset of this scaling behavior probably occurs at much larger chain lengths N.

6   Conclusions

The configurations of flexible polymers endgrafted at the inner walls of cylindrical tubes under good solvent conditions were studied by two complementary approaches, namely by a scaling theory and by Monte Carlo simulation of a bead-spring model.

The scaling treatment can identify the asymptotic power laws of the chain linear dimensions R_{gx}, R_{gy} and R_{gz} and the brush height h in terms of the parameters of the problem, namely the chain length N, the grafting density σ, and the tube diameter D. These power laws, however, are valid only asymptotically in the limit $N \to \infty$, keeping the scaled grafting density $\tilde{\sigma} = \sigma N^{6/5}$ and the scaled tube diameter $\tilde{D} = DN^{-3/5}$ fixed. In this limit, also the scaled linear dimensions $\tilde{R}_{g\alpha} = R_{g\alpha}N^{-3/5}$ ($\alpha = x, y, z$) and $\tilde{h} = hN^{-3/5}$ will not exhibit any explicit dependence on N any more, but will depend on the scaled variables $\tilde{\sigma}$ and $\tilde{D}$ only (see Fig. 4, for example).

It should be noted, that even in this limit the scaling theory is grossly oversimplified, since the different regimes that have been identified (mushrooms, cigars; compressed cigars; overlapping cigars; compressed brush; normal brush) are not separated by any sharp boundaries, but rather the different power laws that characterize these regimes merge gradually by smooth crossovers. These crossover regions may extend over several decades of the appropriate control variable (such as $\tilde{\sigma}$). Therefore the lines in the "state diagram" of the polymer brush (Fig. 3) should not be mixed up with lines appearing in a thermodynamic phase diagram: here the lines only mark the center of the crossover region (fig. 3), and all the kinks in a scaling diagram such as Fig. 4 are rounded off. However, we are not aware of any analytical method that could provide the functions that describe these smooth crossovers.

Real polymer brushes confined in such a cylindrical pore geometry will hardly obey these rather stringent conditions under which the scaling considerations are strictly applicable, and the same caveat holds for computer simulations. Nevertheless the scaling approach is useful as a first guidance towards this rather complex behavior.

The Monte Carlo simulations yield not only the gyration radius components of the chains, but also the full density profiles of the monomers, the distribution function of the chain ends, etc. It has been found that the chain ends are distributed all over the cylindrical tube, if the monomer density inside the tube gets large. While for brushes on planar substrates chain end distributions still have a broad maximum located roughly near the brush height, in the cylindrical geometry these distributions are much broader. It is also remarkable that this distribution spans the full range of radial distances ($0 < r' < D$), rather than being restricted only to the region from the grafting point to the cylinder axis (Fig. 2), $0 < r' < D/2$. Our findings imply that theories that approximate the chain end distribution by a delta function $\delta(r' - h)$ cannot be trusted. Thus, we identify cases where the brush height in the cylinder increases when the cylinder radius is decreased, in contrast to predictions of such theories. This means that for smaller D we find that the curvature slightly enhances chain stretching in the direction normal to the grafting substrate, but this effect is rather small.

Due to technical difficulties of preparing well-equilibrated configurations of polymer brushes in cylindrical pores, only rather short chains could be studied, which do not allow a decisive test of the scaling theory yet. Nevertheless the scaling theory does provide a useful framework to analyze and discuss the Monte Carlo results.

In future work, we plan to consider transport through such polymer-coated nanopipes. We also hope that our study will stimulate experimental work on such cylindrical brushes. Also a detailed comparison to self-consistent field treatments would be valuable.
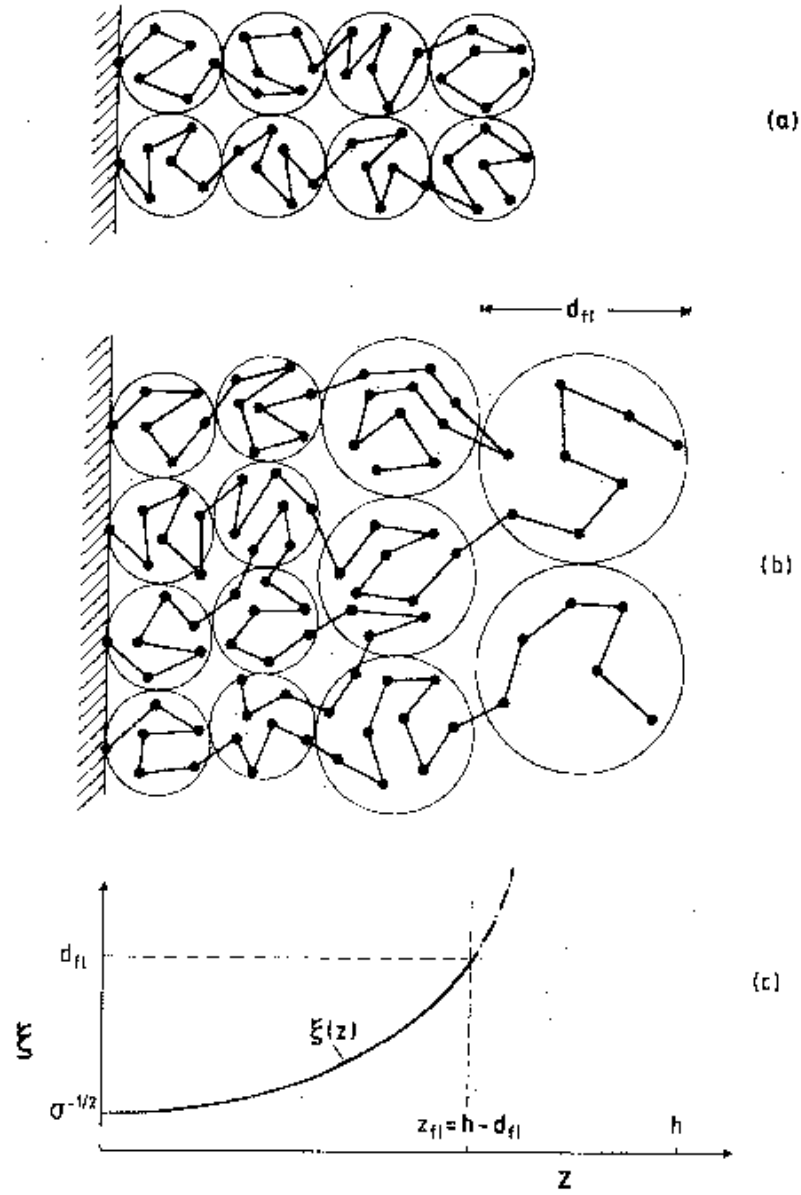
Figure 1: Blob picture of a polymer brush grafted on a flat substrate in the good solvent regime. (a) Alexander-de Gennes model: the chains are treated as linear "cigars" of blobs with uniform diameter $\xi = \sigma^{-1/2}$, σ being the grafting density [9, 10]. (b) Non-uniform blob picture [6]: consistent with a decrease of the monomer density $\phi(z)$ in the brush with increasing distance z from the grafting substrate surface, the blob diameter (which can also be interpreted as the screening length ξ of excluded volume interactions, see (c)) increases with the distance z.
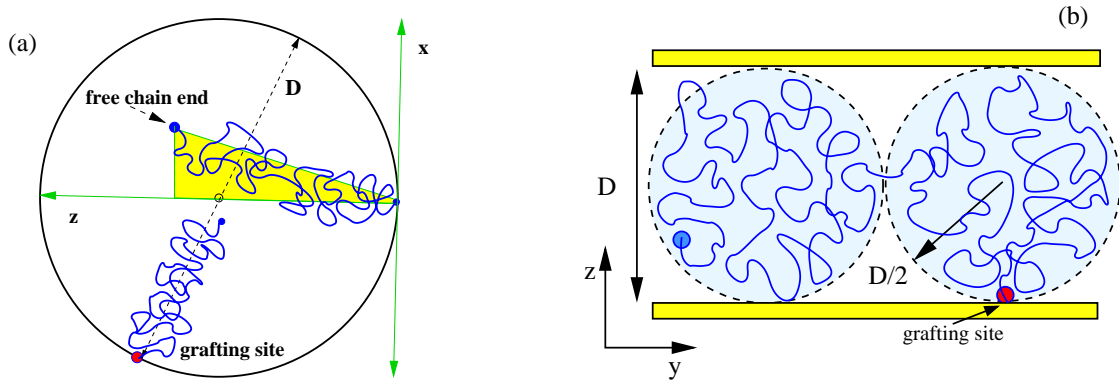
Figure 2: (a) Choice of coordinates in a cylindrical tube of diameter D used for the analysis of the gyration radius components of the chains grafted on the interior pore surface. For each polymer chain a separate coordinate system is chosen with the origin at the grafting site whereby the z-axis is oriented perpendicular to the grafting surface and points towards the tube axis. The y-axis is parallel to the tube axis, and the x-axis is normal to both other axes in the tangential plane at the grafting site. Note that z-coordinates larger than $D/2$ are possible. This coordinate system is also used to study the distribution $\phi(\vec{r})$ of the monomers and $\rho(\vec{r})$ of the free chain ends. (b) Schematic blob picture of a "cigar", describing the state of a chain in a narrow tube in the dilute limit.
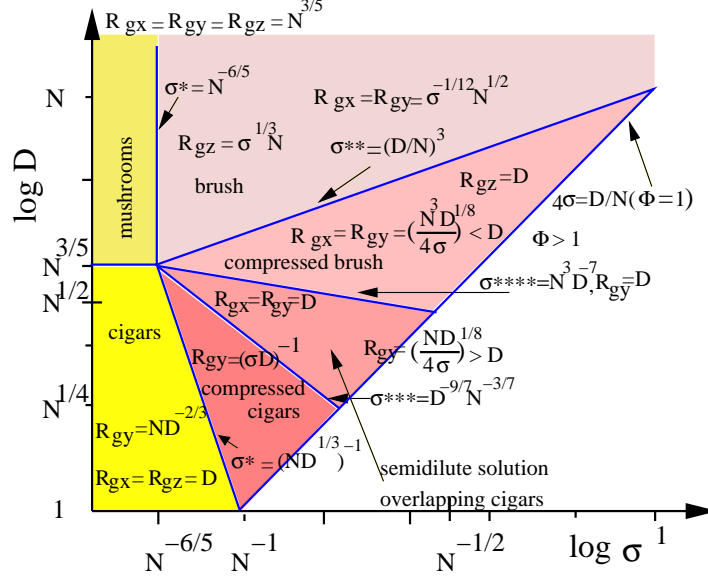
Figure 3: Schematic diagram for the dimensions of a chain of length N in terms of tube diameter D and grafting density σ. Straight lines indicate the crossovers between the various scaling regimes. For *wide* tubes ($D > N^{3/5}$) with increasing σ only two crossovers are encountered: at $\sigma = \sigma^* = N^{-6/5}$ from mushrooms to a quasi-flat brush, and then at $\sigma^{**} = (D/N)^3$ to a compressed brush. The latter regime ends at $\sigma = (1/4)D/N$, where the tube is densely filled with monomers ($\phi = 1$). Since the line, corresponding to $\phi = 1$ (the regime $\phi > 1$ is unphysical) meets the line σ^{**} at $D = N$, for $D > N$ no compressed brush exists any longer. For *narrow* tubes, $D < N^{3/5}$, instead of mushrooms one has cigars, elongated along the tube axis. Three sub-regimes need to be distinguished: For moderately narrow tubes, $N^{1/2} < D < N^{3/5}$, three successive crossovers are distinguished: At $\sigma = \sigma^* = (ND^{1/3})^{-1}$ a crossover from *swollen* cigars to *compressed* non-overlapping cigars occurs. At $\sigma^{***} = D^{-9/7}N^{3/7}$ these cigars start to overlap strongly whereby for $\sigma^{***} < \sigma < \sigma^{****} = N^3 D^{-7}$ their linear dimension in y-direction still exceeds the tube diameter. At σ^{****} the chains behave similar as in a bulk semidilute solution of the same density and $R_{gy} = D$. For $\sigma > \sigma^{****}$, the regime of the compressed brush (as described for $D > N^{3/5}$) is entered again. For narrow tubes, $N^{1/4} < \sigma < N^{1/2}$, the latter regime no longer exists, however. Finally, for *ultranarrow* tubes ($1 < D < N^{1/4}$) only a single crossover from swollen to laterally compressed cigars is possible.
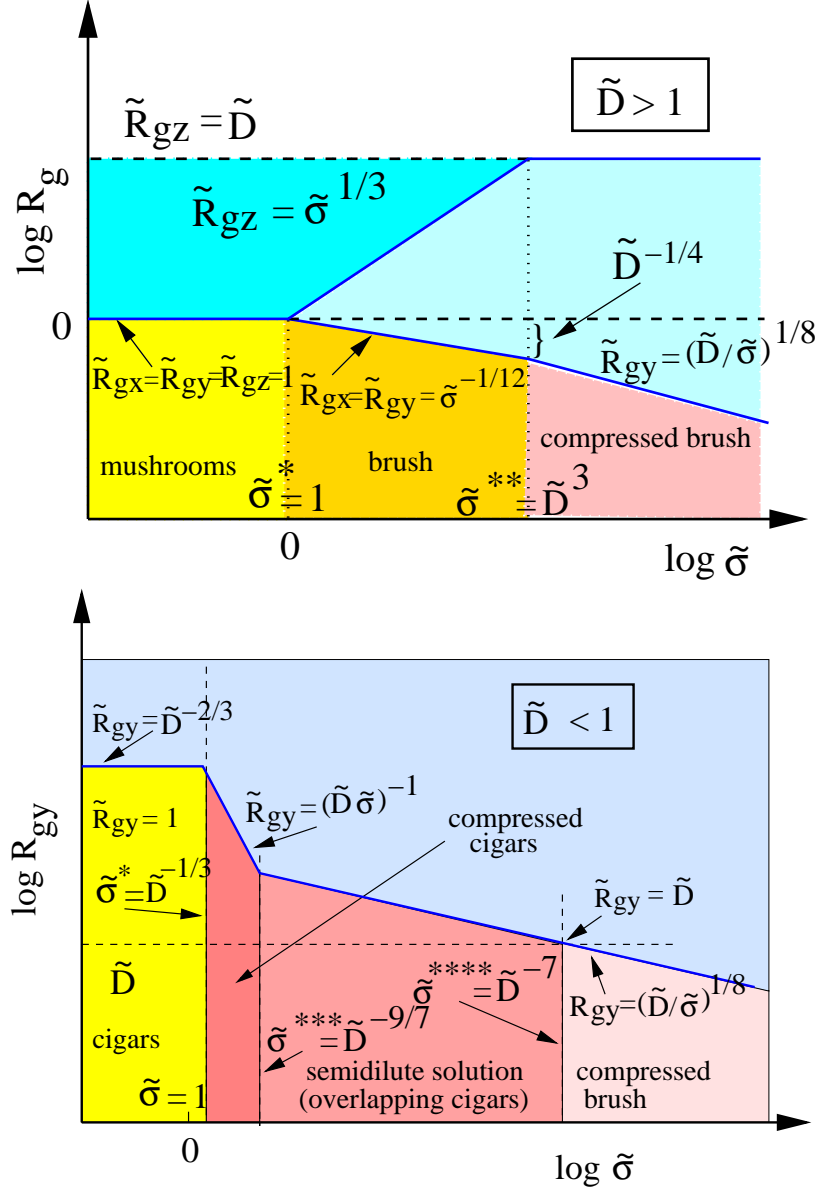
Figure 4: Schematic variation of the scaled linear dimensions $\tilde{R}_{gy} = R_{gy}/N^{3/5}$, $\tilde{R}_{gz} = R_{gz}/N^{3/5}$ with the scaled grafting density $\tilde{\sigma} = \sigma N^{6/5}$ on a log-log plot. For wide tubes ($\tilde{D} > 1$, upper part) and moderately narrow tubes ($\tilde{D} < 1$ but $D > N^{1/2}$, lower part) there is no longer any dependence on chain length N. Since the crossovers at the various grafting densities $\tilde{\sigma}^*$, $\tilde{\sigma}^{**}$, $\tilde{\sigma}^{***}$ and $\tilde{\sigma}^{****}$ are not sharp, the dashed vertical straight lines should be understood as centers of crossover regions only, cf. text.
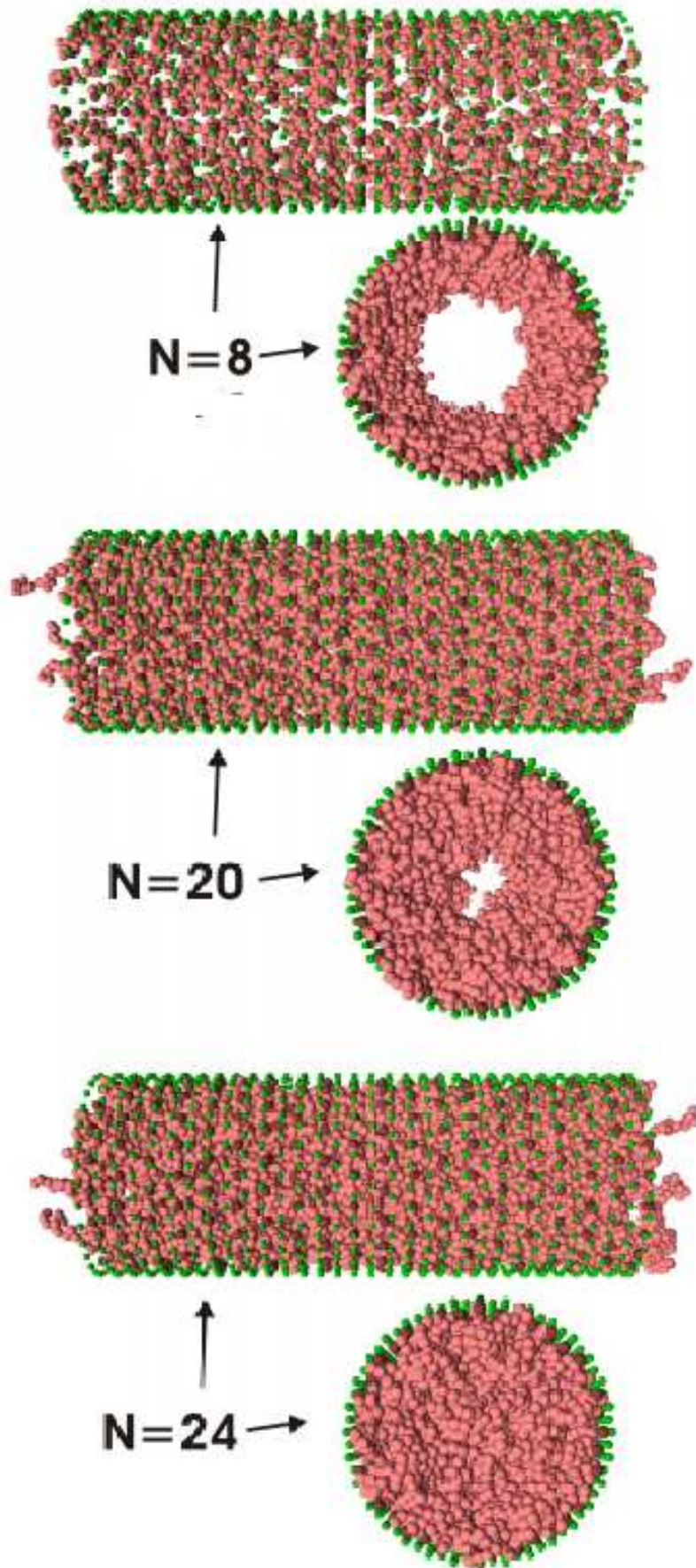
Figure 5: Snapshot configurations of the brush in a tube of diameter $D = 30$ and length $L = \pi D$, for three choices of N: $N = 8$ (upper part), $N = 20$ (middle part) and $N = 24$ (lower part). Both views of the outside and of cross sections are
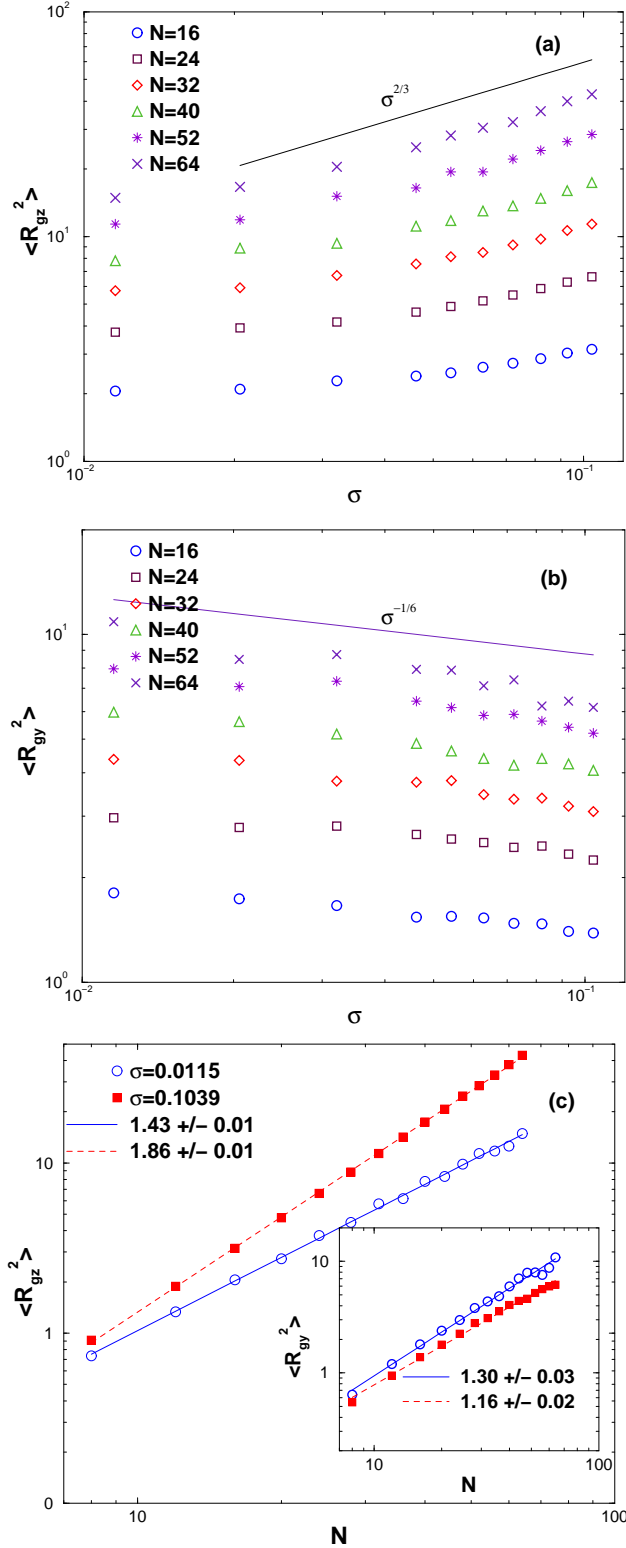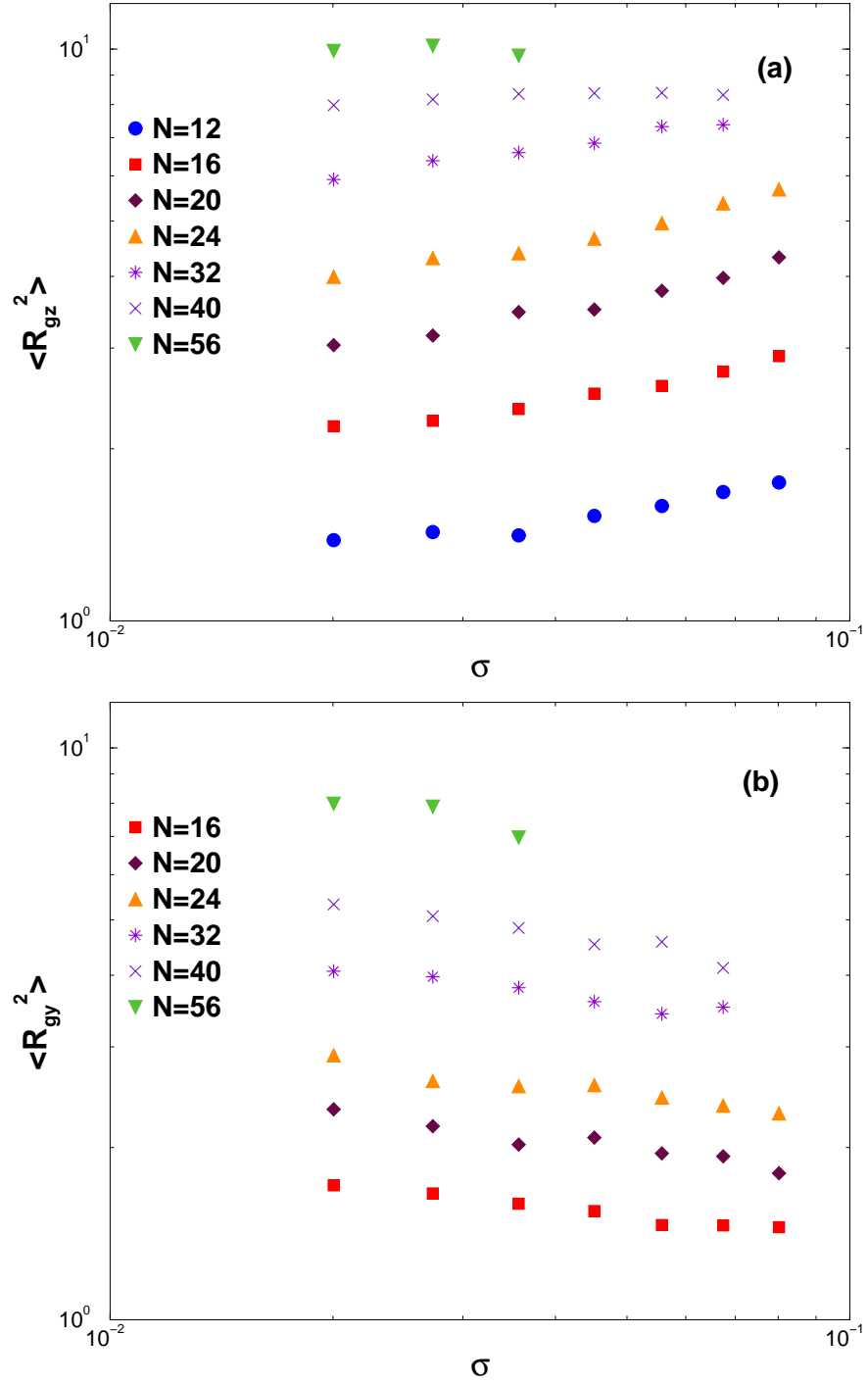
Figure 6: Log-log plot of $\langle R_{gz}^2 \rangle$ (a) and $\langle R_{gy}^2 \rangle$ (b) versus grafting density σ, using a perfectly flat substrate. The total number of chains ranges from 36 ($\sigma = 0.011547$) to 324 ($\sigma = 0.103926$). Chain lengths $N = 16, 24, 32, 40, 52$ and 64 are included in the plot, as indicated. Straight lines indicate the theoretical power laws $\langle R_{gz}^2 \rangle \propto \sigma^{2/3}$ and $\langle R_{gy}^2 \rangle \propto \sigma^{-1/6}$ that apply in the semidilute regime of strongly stretched brushes under good solvent conditions (Eqs. (2), (3)). Upper part of (b) shows a plot of $\langle R_{gy}^2 \rangle$ vs N, while (c) shows a plot of $\langle R_{gz}^2 \rangle$ vs. N.
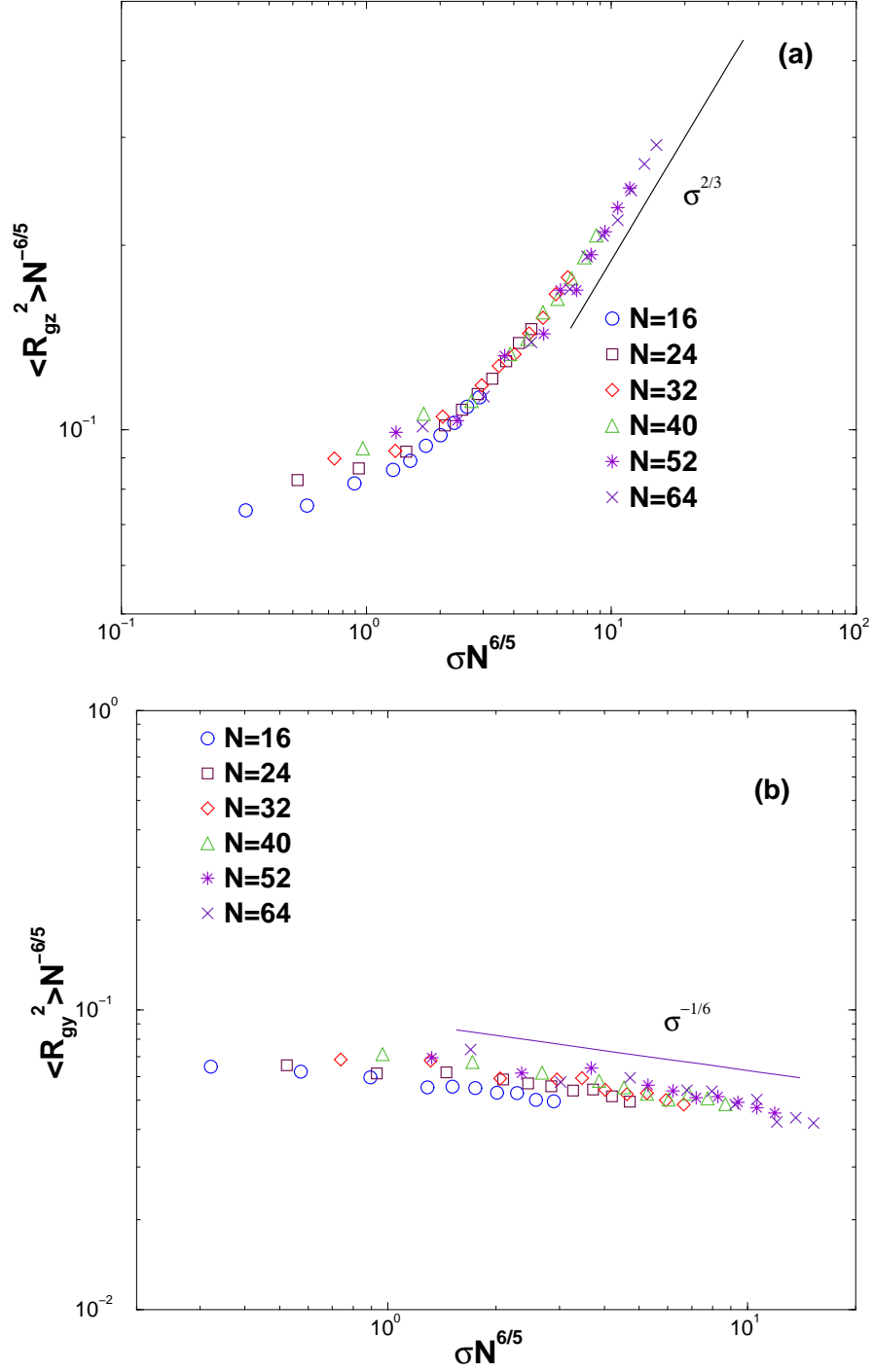
Figure 7: Scaling plots where $\tilde{R}^2_{gz} = \langle R^2_{gz}\rangle/N^{6/5}$ (a) and $\tilde{R}^2_{gy} = \langle R^2_{gy}\rangle/N^{6/5}$ (b) are shown as functions of the scaled grafting density $\sigma N^{6/5}$, in a log-log representation. Same data as shown in Fig. 6 are used, and again the theoretical power laws $\tilde{R}^2_{gz} \propto \tilde{\sigma}^{2/3}$ and $\tilde{R}^2_{gy} \propto \tilde{\sigma}^{-1/6}$ are indicated by straight lines.

Figure 8: Log-log plot of $\langle R_{gz}^2 \rangle$ (a) and $\langle R_{gy}^2 \rangle$ (b) versus grafting density σ, for a brush in a tube of diameter $D = 30$. The total number of chains ranged from 144 ($\sigma = 0.02$) to 576 ($\sigma = 0.08$). For $\sigma \leq 0.0356$ chain lengths $N = 12, 16, 20, 24, 32, 40$ and 56 are included, while for larger σ some of the larger chain lengths needed to be omitted since melt densities were reached inside the pore (recall Fig. 3: the unphysical regime cannot be entered).
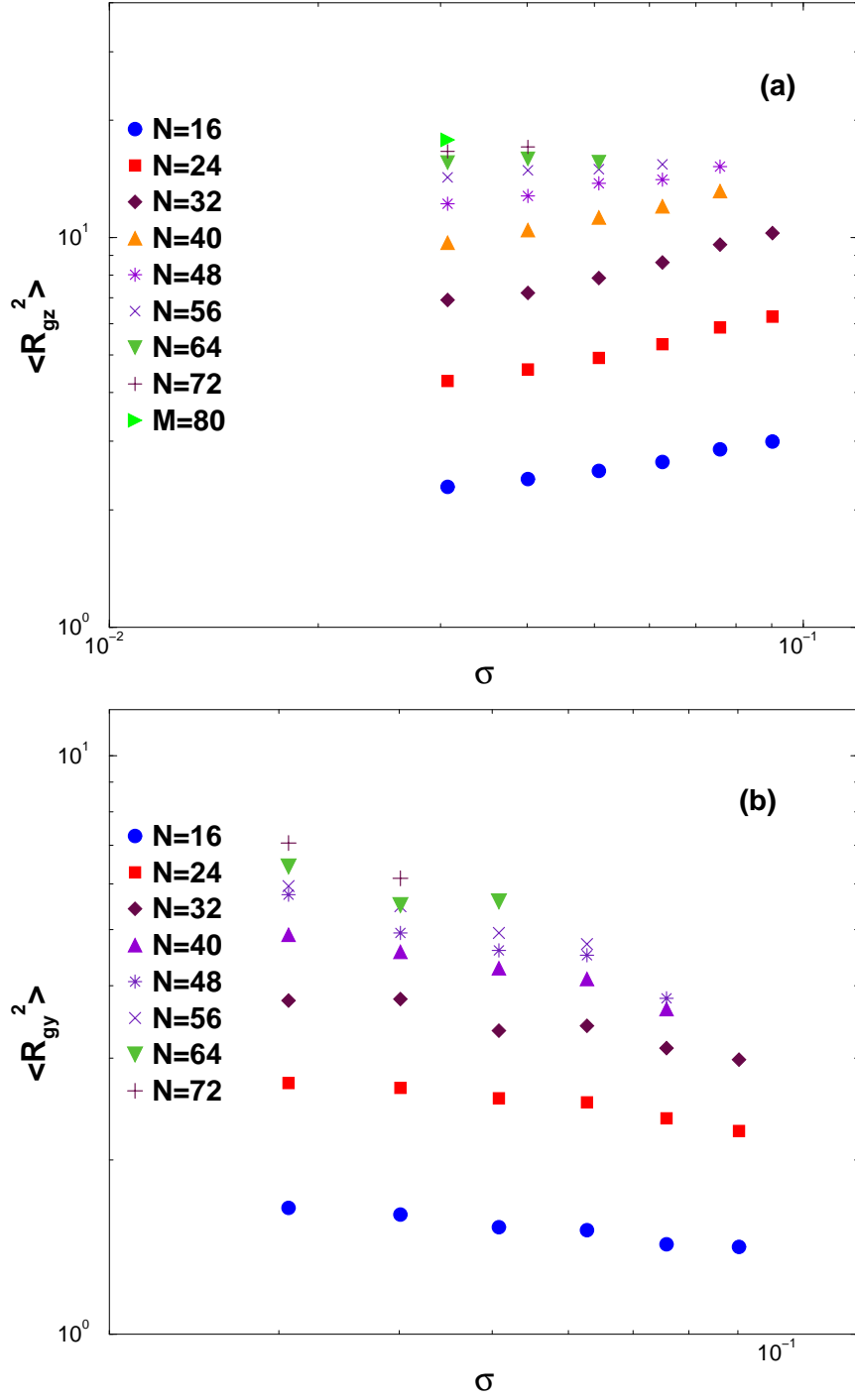
Figure 9: Same as Fig. 8, but for $D = 42$. The total number of chains ranges from 294 ($\sigma = 0.031$) to 864 ($\sigma = 0.09$). Chain lengths up to $N = 80$ are included for the smallest and up to $N = 32$ for the largest grafting density.
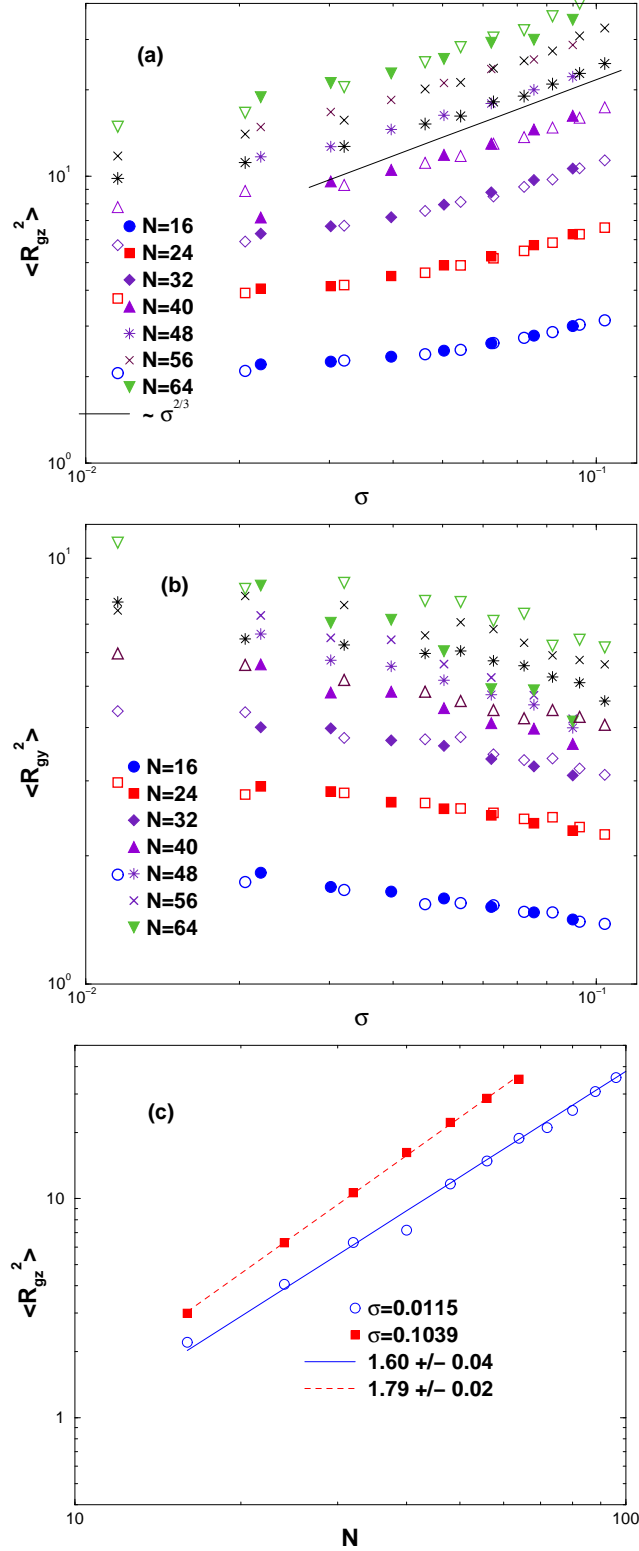
Figure 10: Same as Fig. 8, but for $D = 62$. The total number of chains ranges from 280 ($\sigma = 0.022$) to 1144 ($\sigma = 0.09$). Part (c) shows a log-log plot of $\langle R_{gz}^2 \rangle$ vs. N for two grafting densities. In parts (a), (b) we have included corresponding data for the flat brush on $\langle R_{gz}^2 \rangle$ (empty symbols) to show that at least for $N = 32$ and $N = 40$ the chains for the brush in the tube are slightly more stretched than for the flat brush.
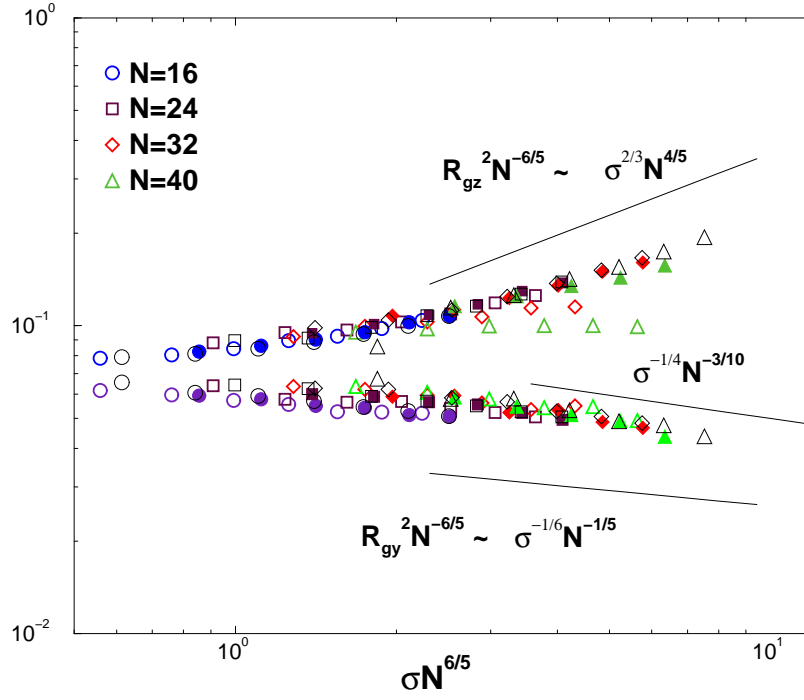
Figure 11: Scaling representation where $\tilde{R}_{gz}^2$ (upper part) and $\tilde{R}_{gy}^2$ (lower part) is plotted versus $\tilde{\sigma}$ in double-logarithmic form, including data for various N and D. Open symbols: (thick small) $D = 30$, (thin big) $D = 62$. Full symbols: $D = 42$. Predicted power laws for the brush regime and the regime of the compressed brush are shown by straight lines.
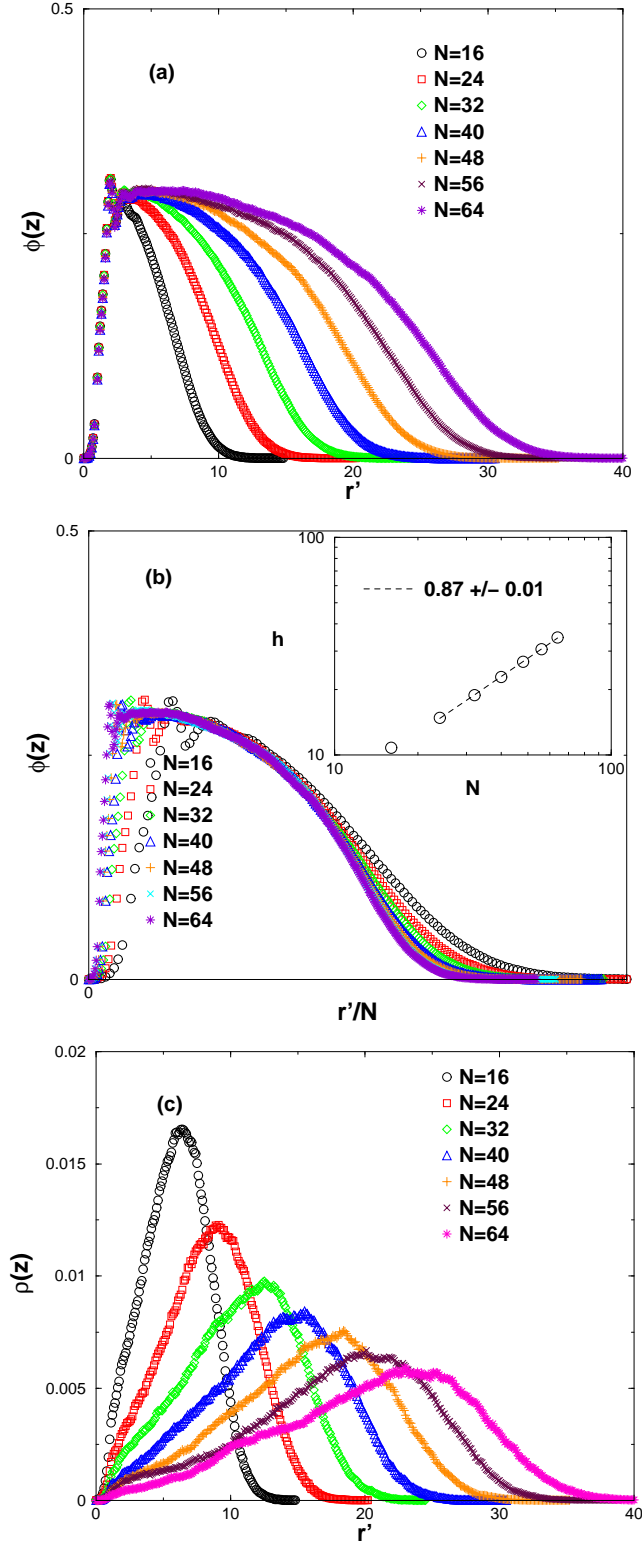
Figure 12: Monomer density profile $\phi(r')$ of a polymer brush on a flat substrate (a) and plotted versus the rescaled distance r'/N (b). All data refer to a grafting density $\sigma = 0.1$ ($N_{ch} = 324$ chains grafted to an area $A = 3117.6$). Seven chain lengths N are included in the figure, as indicated. The insert in the lower part shows a log-log plot of the brush height h versus chain length N. The distribution of free chain ends is shown in (c).
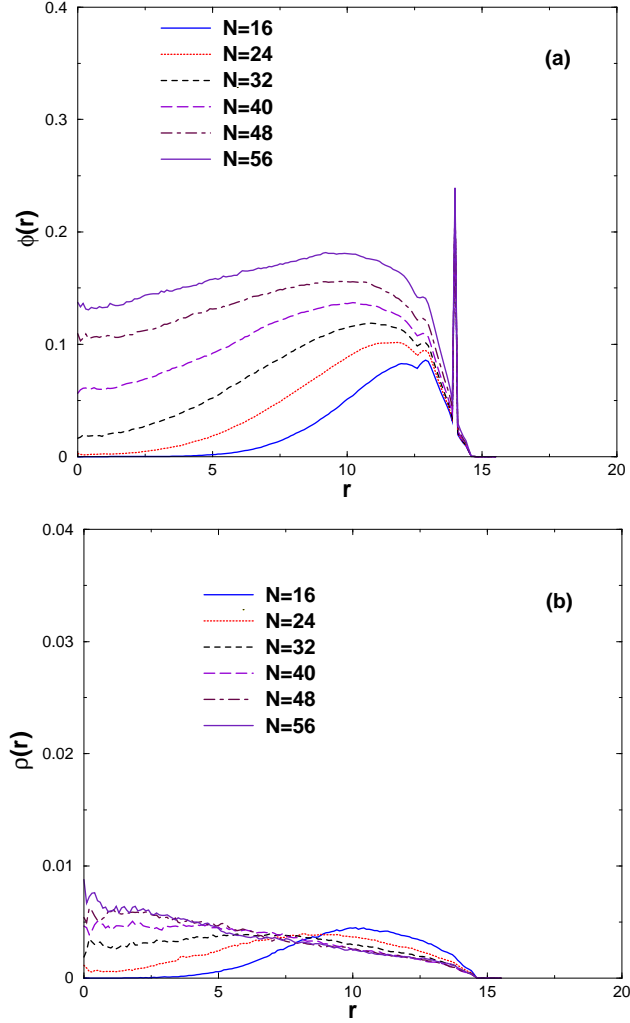
Figure 13: Radial density distribution function $\phi(r)$ of the monomers as a function of the distance r from the cylinder axis, for a tube of radius $R = 15$, at a grafting density $\sigma = 0.02$ ($N_{ch} = 144$ chains), upper part, and the end monomer density distribution, lower part. Remember that at $r = R - 1 = 14$ the first monomer of each grafted chain is located, while the atoms forming the wall are located at $r = R = 15$.
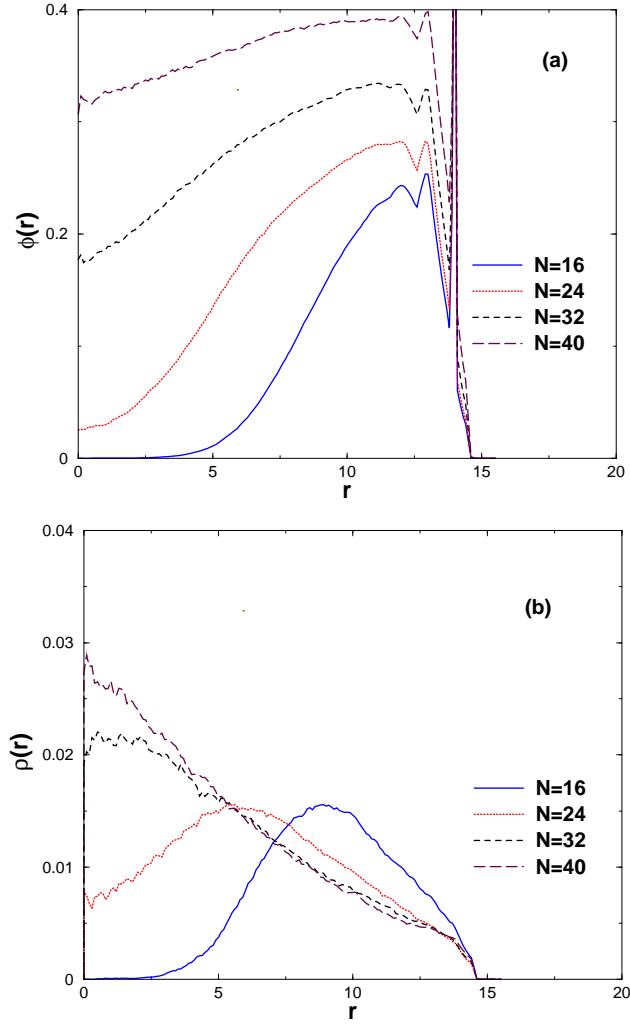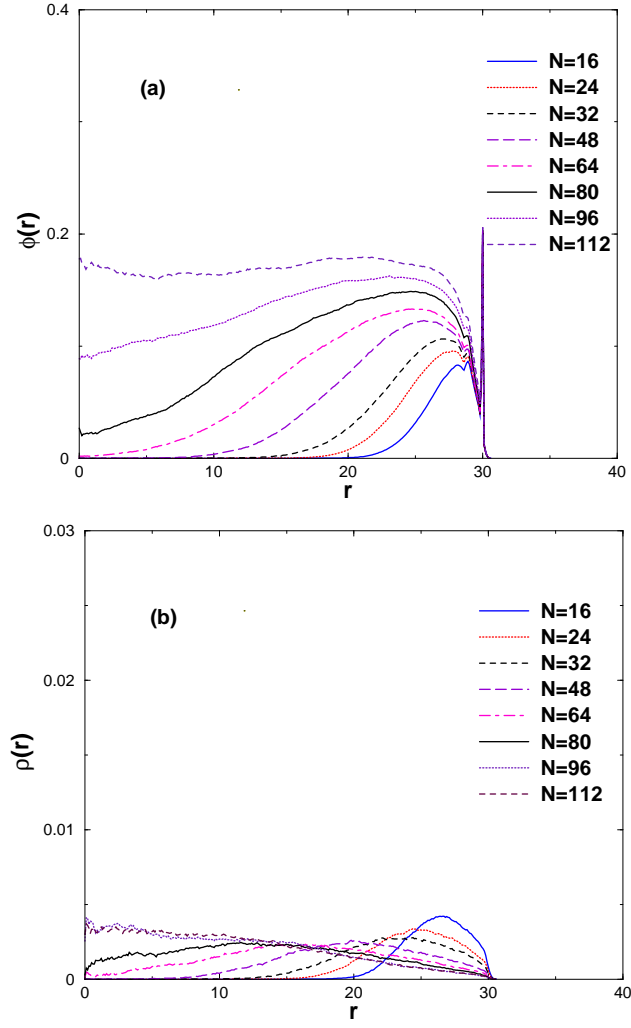
Figure 14: Same as Fig. 14, but for $\sigma = 0.0674$ ($N_{ch} = 484$)

Figure 15: Same as Fig. 14, but for R = 31, $\sigma = 0.022$ ($N_{ch} = 280$)
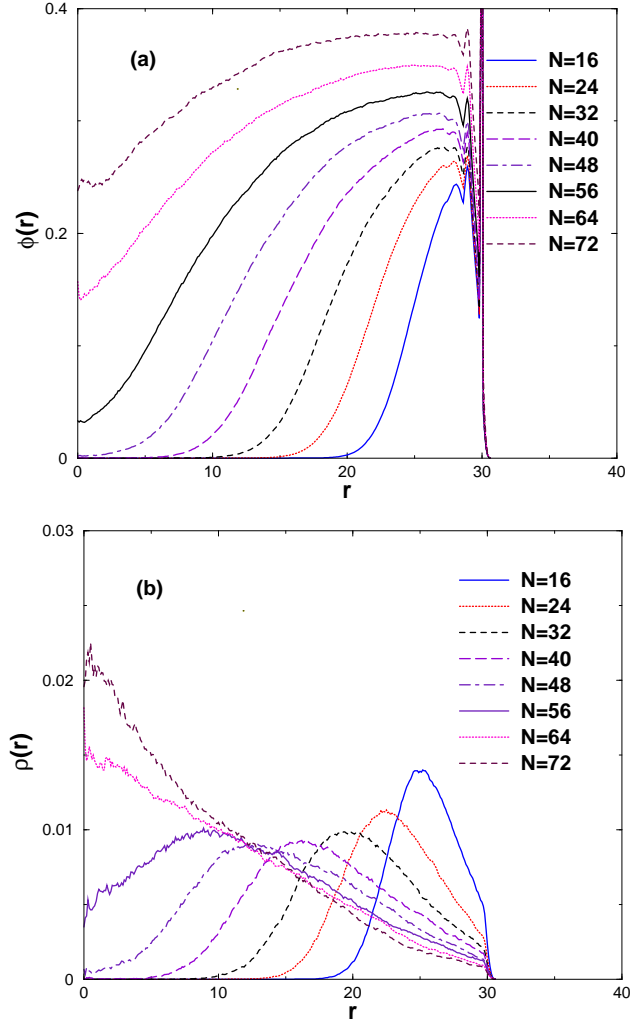
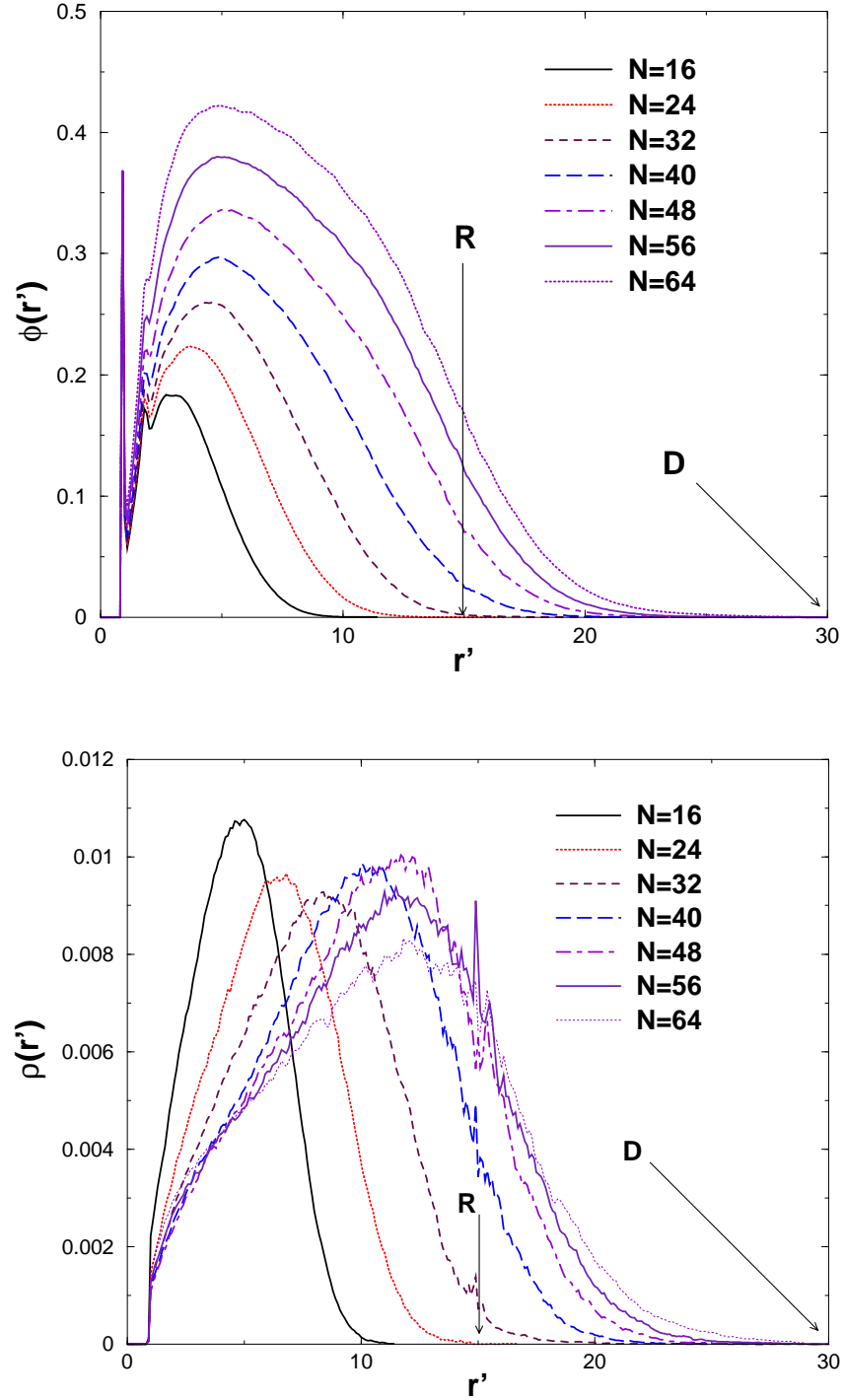Figure 16: Same as Fig. 14, but for R = 31, $\sigma = 0.0755$ ($N_{ch} = 960$)

Figure 17: (a) Density profile $\phi(r')$ of the monomers in the brush for $D = 28$ at the grafting density $\sigma = 0.02$ and various chain lengths. Arrows point to the positions of the cylinder axis and the maximum distance from the grafting site that is possible in z-direction inside the tube are marked by arrows. (b) Distribution $\rho(r')$ of the chain ends, for the same parameters as part (a).
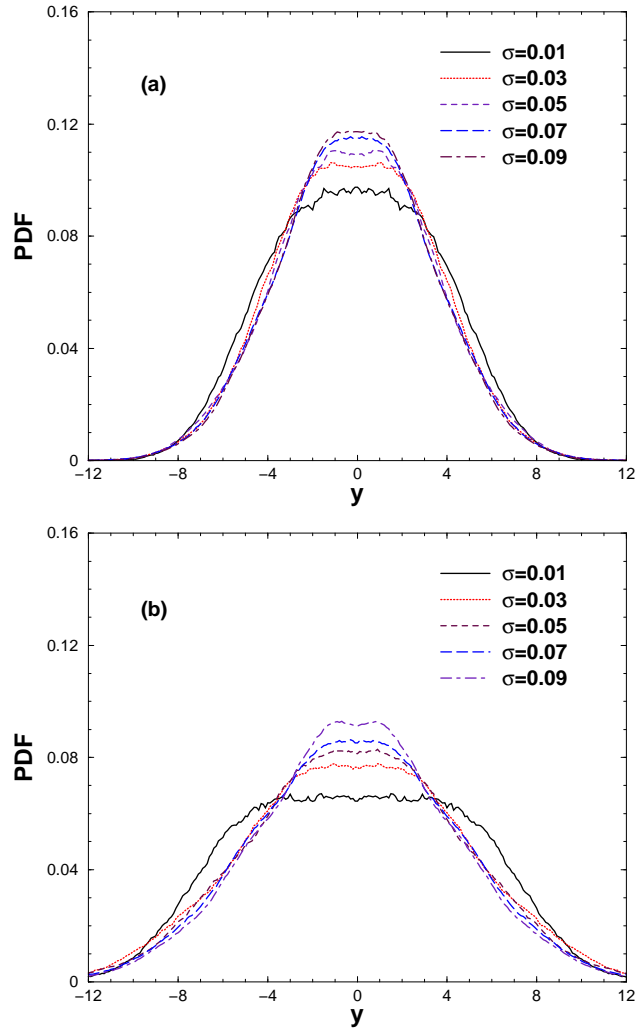
Figure 18: Probability distribution $\rho(y)$ of the chain ends plotted vs. the y-coordinate along the tube axis, for $D = 30$ and two choices of N, $N = 24$ (a) and $N = 40$ (b). Several values of the grafting density are included, as indicated.
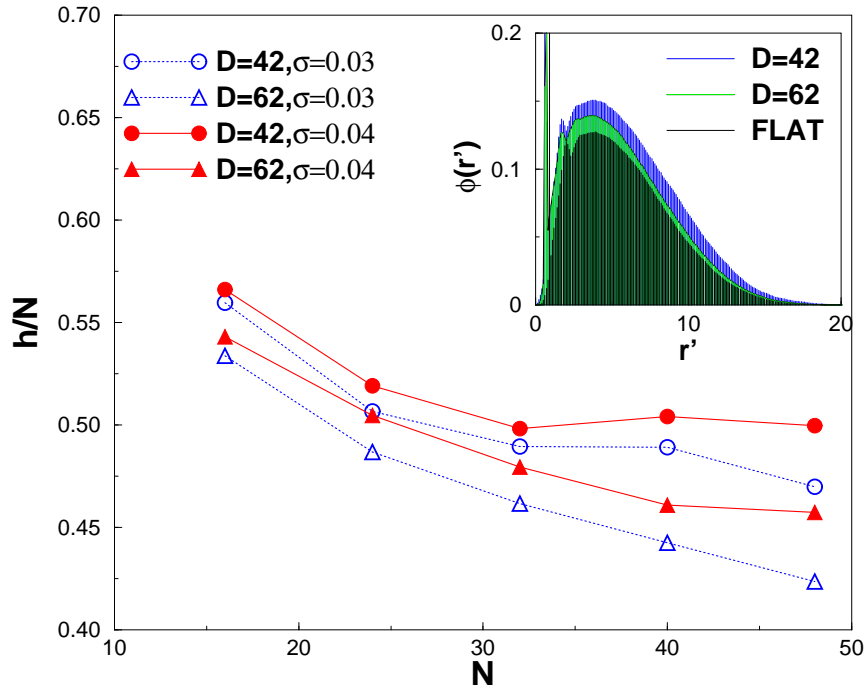
Figure 19: Plot of the reduced brush height h/N in tubes with diameters $D = 42$ and 62 as function of N at two different grafting densities. The inset shows the radial density distribution $\phi(r')$ for $N = 32$ and $\sigma = 0.03$ for a flat substrate (the lowest $\phi(r')$), for a tube with $D = 62$ (intermediate), and for a tube with $D = 42$ (largest $\phi(r')$).

References

[1] A. Halperin, M. Tirrell, and T. P. Lodge, Adv. Polym. Sci. **100**, 31 (1991)

[2] S. T. Milner, Science **251**, 905 (1991)

[3] G. S. Grest and M. Murat, in *Monte Carlo and Molecular Dynamics Simulations in Polymer Science*, edited by K. Binder (Oxford University Press, New York, 1995), pp. 476-578.

[4] G. S. Grest, Adv. Poly. Sci. **138**, 149 (1999)

[5] R. C. Advincula, W. J. Brittain, K. C. Caster, and J. Rühe (eds.) *Polymer Brushes* (Wiley-VCH, Weinheim 2004)

[6] J. Wittmer, A. Johner, J.-F. Joanny and K. Binder, J. Chem. Phys. **101**, 4379 (1994)

[7] K. Binder, P.-Y. Lai, and J. Wittmer, Faraday Discuss. **98**, 97 (1994)

[8] K. Binder, Eur. Phys. J. E**9**, 293 (2002)

[9] S. Alexander, J. Phys. (France) **38**, 983 (1977)

[10] P. G. de Gennes, Macromolecules **13**, 1069 (1980)

[11] A. N. Semenov, Sov. Phys. JETP Lett. **61**, 733 (1985)

[12] S. T. Milner, T. A. Witten, and M. E. Cates, Europhys. Lett. **5**, 413 (1988); Macromolecules **21**, 2610 (1988); S. T. Milner, Z. G. Wang and T. A. Witten, Macromolecules **22**, 489 (1989)

[13] A. M. Skvortsov, A. A. Gorbunov, V. A. Pavlushkov, E. B. Zhulina, O. V. Borisov, and V. A. Pryamitsyn, Polym. Sci. USSR Ser. A.**30**, 1706 (1988); E. B. Zhulina, O. V. Borisov, and V. A. Pryamitsyn, J. Colloid Interface Sci. **137**, 495 (1990)

[14] E. B. Zhulina, V. A. Pryamitsyn, and O. V. Borisov, Polymer Sci. USSR Ser. A**31**, 205 (1989); E. B. Zhulina, O. V. Borisov, V. A. Pryamitsyn, and T. M. Birshtein, Macromolecules **24**, 140 (1991)

[15] M. Murat and G. S. Grest, Phys. Rev. Lett. **63**, 1074 (1989); Macromolecules **22**, 4054 (1989)

[16] A. Chakrabarti and R. Toral, Macromolecules **23**, 2016 (1990)

[17] P.-Y. Lai and K. Binder, J. Chem. Phys. **95**, 9288 (1991)

[18] T. Kreer, S. Metzger, M. Müller, K. Binder and J. Baschnagel, J. Chem. Phys. **120**, 4012 (2004)

[19] C. M. Wijmans and E. B. Zhulina, Macromolecules **26**, 7214 (1993)

[20] E. M. Sevick, Macromolecules **29**, 6952 (1996)

[21] E. N. Govorun and I. Erukhimovich, Langmuir **15**, 8392 (1999)

[22] K. Prochazka, J. Phys. Chem. **99**, 14108 (1995)

[24] N. Dan and M. Tirrell, Macromolecues **26**, 637 (1993)

[25] C. Hiergeist and R. Lipowsky, J. Phys. II France **6**, 1465 (1996)

[26] P. Sotta, A. Lesne and J. M. Victor, J. Chem. Phys. **112**, 1565 (2000)

[27] M. Daoud and P. G. de Gennes, J. Phys. (France) **38**, 85 (1977)

[28] K. Kremer and K. Binder, J. Chem. Phys. **81**, 6381 (1984)

[29] F. Tessier and G. W. Slater, Macromolecules **38**, 6752 (2005)

[30] F. Brochard and P. G. de Gennes, J. Phys. (France) **40**, L399 (1979)

[31] J. Lal, S. Sinha, and L. J. Auvray, J. Phys. II France **7**, 1597 (1997)

[32] S. Jorge and A. Rey, J. Chem. Phys. **108**, 5720 (1997)

[33] I. Teraoka and P. Cifra, Polymer **43**, 3025 (2002)

[34] I. Teraoka and Y. Wang, Polymer **45**, 3825 (2004)

[35] P. G. de Gennes, *Scaling Concepts in Polymer Physics* (Cornell University Press, Ithaca, N. Y. 1979)

[36] P. J. Flory, *Principles of Polymer Chemistry* (Cornell University Press, Ithaca, N. Y. 1953)

[37] A. D. Sokal, in *Monte Carlo and Molecular Dynamics Simulations in Polymer Science* (K. Binder, ed.), p. 47 (Oxford Univ. Press, N. Y., 1995)

[38] J. Zinn-Justin, Phys. Rep. **344**, 159 (2001)

[39] K. Binder, in *Computational Modeling of Polymers*, edited by J. Bicerano (Marcel Dekker, N. Y., 1992) p. 221

[40] K. Binder (ed.) *Monte Carlo and Molecular Dynamics Simulations in Polymer Science* (Oxford University Press, New York, 1995)

[41] K. Binder and G. Ciccotti (eds.) *Monte Carlo and Molecular Dynamics of Condensed Matter Systems* (Societa Italiana di Fisica, Bologna, 1996)

[42] K. Binder and A. Milchev, J. Computer-Aided Mater. Design **9**, 33 (2000)

[43] M. Kotelyanskii and D. N. Theodorou (eds.) *Computer Simulation Methods for Polymers* (M. Dekker, N. Y., 2004)

[44] G. S. Grest and K. Kremer, Phys. Rev. A**33**, 3628 (1986); K. Kremer and G. S. Grest, J. Chem. Phys. **92**, 5057 (1990)

[45] C. Bennemann, K. Binder, W. Paul and B. Dünweg, Phys. Rev. E**57**, 843 (1998)

[46] K. Binder, J. Baschnagel, and W. Paul, Progr. Polym. Sci. **28**, 115 (2005)

[47] M. Müller and L. G. MacDowell, Macromolecules **33**, 3902 (2000)

[48] G. S. Grest and M. Murat, Macromolecules **26**, 3108 (1993)

[49] T. Kreer, M. H. Müser, K. Binder, and J. Klein, Langmuir **17**, 7804 (2001); T. Kreer, M. H. Müser, and K. Binder, Langmuir **19**, 7551 (2003)

[50] D. Frenkel and B. Smit, *Understanding Molecular Simulations. From Algorithms to Aplications* (Academic Press, San Diego, 2002)

[51] G. J. Fleer, M. A. Cohen Stuart, J. M. H. M. Scheutjens, T. Cosgrove and B. Vincent, *Polymers at Interfaces* (Chapman and Hall, London, 1993)

[52] T. Cosgrove, T. Heath, B. van Lent, F. Leermakers, and J. M. H. M. Scheutjens, Macromolecules **20**, 1692 (1988); B. van Lent, R. Israels, J. M. H. M. Scheutjens, and G. J. Fleer, J. Colloid Interface Sci. **137**, 380 (1990); C. M. Wijmans, J. M. H. M. Scheutjens, and E. B. Zhulina, Macromolecules **25**, 2657 (1992)

[53] S. T. Milner and T. A. Witten, J. Phys. (Paris) **49**, 1951 (1988)